
Spectroscopic Properties of Polarons in Strongly Correlated Systems by Exact Diagrammatic Monte Carlo Method

A. S. Mishchenko^{1,2} and N. Nagaosa³

¹ CREST, Japan Science and Technology Agency (JST), AIST, 1-1-1, Higashi, Tsukuba 305-8562, Japan.

² Russian Research Centre “Kurchatov Institute”, 123182 Moscow, Russia.

³ Department of Applied Physics, The University of Tokyo, 7-3-1 Hongo, Bunkyo-ku, Tokyo 113, Japan.

1 Introduction

Theoretical study of polarons in the strongly correlated system is like an attempt to view contents of a Pandora box embedded into another, even more sinister and obscure, container of riddles, enigmas and mysteries. This desperate situation occurs because solution is not known even for the simplest polaron problem, i.e. when a perfectly stable quasiparticle (QP) with momentum as a single quantum number interacts with a well defined bath of bosonic elementary excitations. To the contrary, the definition of the strongly correlated system implies that QPs might be highly unstable and the very notion of QPs, both in electronic and bosonic subsystems, is under question. Thus, one faces the problem of an interplay between ill defined objects and it is crucial to solve the problem without approximations. Further difficulty, pertinent to realistic systems, is an interplay of the momentum and other quantum numbers characterizing internal states of a QP.

The problem of polaron originally emerged as that of an electron coupled to phonons (see [1, 2]). In the initial formulation a structureless QP is characterized by the only quantum number, momentum, which changes due to interaction of the QP with phonons [3, 4]. Later, depending on what can be called “particle” and “environment”, and how they interact with each other, the polaron concept was related to extreme diversity of physical phenomena. There are many other objects which, having nothing to do with phonons, are isomorphic to simple polaron [5], as, e.g. an exciton-polaron in the intraband scattering approximation [6, 7, 8, 9]. Another example is the problem of a hole in the antiferromagnet which is closely related to polaron since hole movement is accompanied by the spin flips which, in the spin wave approximation, are equivalent to creation and annihilation of magnons [10, 11].

The concept of polaron was further generalized to include internal degrees of freedom which, interacting with environment, change their quantum numbers. Example of a complex QP is the Jahn-Teller polaron, where electron-phonon interaction (EPI) changes quantum numbers of degenerate electronic states [12, 13, 14]. This generalization is important due to its relevance to the colossal magnetoresistance phenomena in the manganese oxides [15, 16]. Another example is the pseudo Jahn-Teller polaron, where EPI is inelastic and leads to transitions between close in energy electronic levels of a QP [17, 18, 19]. Further generalization is a system of several QPs which interact both with each other and environment. For example, effective interaction of two electrons through exchange by phonons can overcome the Coulomb repulsion and form a bound state, bipolaron [20, 21, 22, 23, 24]. On the other hand, coupling of attracting hole and electron to the lattice vibrations [25, 26, 27] can create a lot of qualitatively different objects: localized exciton, weakly bound pair of localized hole and localized electron, etc. [28, 7]. Scattering by impurities introduces additional complexity to the polaron problem because interference of impurity potential with lattice distortion, which accompanies the polaron movement, can contribute either constructively or destructively to the localization of a QP on impurity [29, 30, 7].

In addition, a bare QP and bosonic bath can not be considered as well defined in the correlated systems. Angle Resolved Photoemission Spectra (ARPES), revealing the Lehmann Function (LF) of quasiparticle, demonstrate broad peaks in many correlated systems: copper oxide high-temperature superconductors [31, 32, 33], colossal magnetoresistive manganites [34, 35, 36], quasi-one-dimensional Peierls conductors [37, 38], and Verwey magnetites [39]. Besides, phonons are also broadened in many correlated systems, e.g. in high-temperature semiconductors [40] and mixed-valent materials [41, 42]. One of possible reasons for these broadenings is the interaction of the QPs with the lattice degrees of freedom. However, in many realistic cases other subsystems, not explicitly included into the polaron Hamiltonian, are responsible for the decay of QP and phonons, e.g., another electronic bands, phonon anharmonicity, interaction with nuclear spins, etc. Then, if this auxiliary broadening is known in some approximation, one can formulate an ambitious goal to study spectral response when “bare” quasiparticle with known damping interacts with “broadened” bosonic excitations.

No one of traditional numerical methods, to say nothing of analytical ones, can give *approximation free results for measurable quantities* of polaron, such as optical conductivity or angle resolved photoemission spectra, for *in macroscopic system of arbitrary dimension*. Besides, we are not aware of any numerical method which can incorporate in an approximation free way the information on the damping of QP and bosonic bath. Below we describe basics of recently developed Diagrammatic Monte Carlo (DMC) method for numerically exact computation of Green functions and correlation functions in imaginary time for few polarons in a macroscopic system [43, 44, 45, 46, 47, 48, 49, 50, 51]. Analytic continuation of imaginary time functions to real frequencies is per-

formed by a novel approximation free approach of stochastic optimization (SO) [45, 50, 51], circumventing difficulties of popular Maximal Entropy method. Finally we focus on results of application of the DMC-SO machinery to various problems [52, 53, 54, 55, 56, 57]

The basic models, related to the polaronic objects in correlated systems, which can be solved by DMC-SO methods, are stated in the next Sect. It is followed in Sect. 1.2 by description of stumbling blocks encountered by analytic methods. Sect. 2 concerns the basics of DMC-SO methods. However, those who are not interested in the details of the methods can briefly look through the definitions in the introduction for Sect. 2 and turn to Sect. 3 where LF and optical conductivity of Fröhlich polaron are discussed (see also [58]). Results of studies of the self-trapping phenomenon are presented in Sect. 4 and application of DMC-SO methods to the exciton problem can be found in Sect. 5. The chapter is completed by Sect. 6 devoted to studies of ARPES of high temperature superconductors.

1.1 Formulation of a General Model with Interacting Polarons

In general terms, the simplest problem of a complex polaronic object, where center-of-mass motion does not separate from the rest of degrees of freedom, is introduced as system of two QPs

$$\hat{H}_0^{\text{par}} = \sum_{\mathbf{k}} \varepsilon_a(\mathbf{k}) a_{\mathbf{k}}^\dagger a_{\mathbf{k}} + \sum_{\mathbf{k}} \varepsilon_h(\mathbf{k}) h_{\mathbf{k}} h_{\mathbf{k}}^\dagger \quad (1)$$

($a_{\mathbf{k}}$ and $h_{\mathbf{k}}$ are annihilation operators, and $\varepsilon_a(\mathbf{k})$ and $\varepsilon_h(\mathbf{k})$ are dispersions of QPs), which interact with each other

$$\hat{H}_{\text{a-h}} = -N^{-1} \sum_{\mathbf{p}\mathbf{k}\mathbf{k}'} \mathcal{U}(\mathbf{p}, \mathbf{k}, \mathbf{k}') a_{\mathbf{p}+\mathbf{k}}^\dagger h_{\mathbf{p}-\mathbf{k}}^\dagger h_{\mathbf{p}-\mathbf{k}'} h_{\mathbf{p}+\mathbf{k}'}. \quad (2)$$

(N is the number of lattice sites) through the instantaneous Coulomb potential and the scattering by bosons

$$\begin{aligned} \hat{H}_{\text{par-bos}} = & i \sum_{\kappa=1}^Q \sum_{\mathbf{k}, \mathbf{q}} (b_{\mathbf{q}, \kappa}^\dagger - b_{-\mathbf{q}, \kappa}) \\ & \left[\gamma_{aa, \kappa}(\mathbf{k}, \mathbf{q}) a_{\mathbf{k}-\mathbf{q}}^\dagger a_{\mathbf{k}} + \gamma_{hh, \kappa}(\mathbf{k}, \mathbf{q}) h_{\mathbf{k}-\mathbf{q}}^\dagger h_{\mathbf{k}} + \gamma_{ah, \kappa}(\mathbf{k}, \mathbf{q}) h_{\mathbf{k}-\mathbf{q}}^\dagger a_{\mathbf{k}} \right] + h.c. \quad (3) \end{aligned}$$

($\gamma_{[aa, ah, hh], \kappa}$ are interaction constants) where quanta of Q different branches of bosonic excitations are created or annihilated, which are described by

$$\hat{H}_{\text{bos}} = \sum_{\kappa=1}^Q \sum_{\mathbf{q}} \omega_{\mathbf{q}, \kappa} b_{\mathbf{q}, \kappa}^\dagger b_{\mathbf{q}, \kappa}. \quad (4)$$

In general, each QP can be a composite one with internal degree of freedom represented by T different states

$$\hat{H}_0^{\text{PJT}} = \sum_{\mathbf{k}} \sum_{i=1}^T \epsilon_i(\mathbf{k}) a_{i,\mathbf{k}}^\dagger a_{i,\mathbf{k}}, \quad (5)$$

which quantum numbers can be also changed due to nondiagonal part of particle-boson interaction

$$\hat{H}_{\text{par-bos}} = i \sum_{\kappa} \sum_{\mathbf{k}, \mathbf{q}} \sum_{i,j=1}^T \gamma_{ij,\kappa}(\mathbf{k}, \mathbf{q}) (b_{\mathbf{q},\kappa}^\dagger - b_{-\mathbf{q},\kappa}) a_{i,\mathbf{k}-\mathbf{q}}^\dagger a_{j,\mathbf{k}} + h.c. \quad (6)$$

Complicated model (1)-(6) is still too far from the cases encountered in strongly correlated systems. Due to coupling of QPs (1) and (5) and bosonic fields (4) to additional degrees of freedom, these excitations are not well defined from the onset. Namely, the dispersion relation of the QP spectrum $\epsilon(\mathbf{k})$ in realistic system is ill-defined. One can speak of a Lehmann Function (LF) [59, 60, 61] of a QP

$$L_{\mathbf{k}}(\omega) = \sum_{\nu} \delta(\omega - E_{\nu}(\mathbf{k})) |\langle \nu | a_{\mathbf{k}}^\dagger | \text{vac} \rangle|^2 \quad (7)$$

, which is normalized to unity $\int_0^{+\infty} d\omega L_{\mathbf{k}}(\omega) = 1$ and can be interpreted as a probability that a QP has momentum \mathbf{k} and energy ω . (Here $\{|\nu\rangle\}$ is a complete set of eigenstates of Hamiltonian \hat{H} in a sector of given momentum \mathbf{k} : $H|\nu(\mathbf{k})\rangle = E_{\nu}(\mathbf{k})|\nu(\mathbf{k})\rangle$.) Only for noninteracting system the LF reduces to delta function $L_{\mathbf{k}}^{\text{NONINT}}(\omega) = \delta(\omega - \epsilon(\mathbf{k}))$ and, thus, sets up dispersion relation $\omega = \epsilon(\mathbf{k})$.

Specific cases of model (1)-(6) describe enormous variety of physical problems. Hamiltonians (1) and (2), in case of attractive potential $\mathcal{U}(\mathbf{p}, \mathbf{k}, \mathbf{k}') > 0$, describe an exciton with static screening [62, 63]. Besides, expressions (1)-(4) describe bipolaron for repulsive interaction [20, 21, 22, 23, 24] $\mathcal{U}(\mathbf{p}, \mathbf{k}, \mathbf{k}') < 0$ and exciton-polaron otherwise [25, 26, 27]. The simplest model for exciton-phonon interaction, when only two ($T = 2$) lowest states of relative electron-hole motion are relevant (e.g. in one-dimensional charge-transfer exciton [64, 65, 66]), is defined by Hamiltonians (4)-(6). The same relations (4)-(6) describe the problems of Jahn-Teller [all ϵ_i in Hamiltonian (5) are the same] and pseudo Jahn-Teller polaron. The problem of a hole in an antiferromagnet in spin-wave approximation is expressed in terms of Hamiltonians (4)-(6) with $Q = 1$ and $T = 1$. When hole also interacts with phonons, one has to take into account one more bosonic branch and set $Q = 2$ in (4) and (6). Finally, the simplest nontrivial problem of a polaron, i.e. of a structureless QP interacting with one phonon branch, is described by noninteracting Hamiltonians of QP \hat{H}_{par} and phonons \hat{H}_{ph}

$$\hat{H}_0 = \sum_{\mathbf{k}} \epsilon(\mathbf{k}) a_{\mathbf{k}}^\dagger a_{\mathbf{k}} + \sum_{\mathbf{q}} \omega_{\mathbf{q}} b_{\mathbf{q}}^\dagger b_{\mathbf{q}}, \quad (8)$$

and interaction term

$$\hat{H}_{\text{int}} = \sum_{\mathbf{k}, \mathbf{q}} V(\mathbf{k}, \mathbf{q})(b_{\mathbf{q}}^{\dagger} - b_{-\mathbf{q}})a_{\mathbf{k}-\mathbf{q}}^{\dagger}a_{\mathbf{k}} + h.c. . \quad (9)$$

The simplest polaron problem, in turn, can be subdivided into continuous and lattice polaron models.

1.2 Limitations of Analytic Methods in Problem of Polarons

Analytic solution for the problem of exciton in a rigid lattice is available only for small radius Frenkel regime [67] and large radius Wannier regime [68]. However, even limits of validity for these approximations are not known. Random phase approximation approaches [62, 63], are capable of obtaining some qualitative conclusions for intermediate radius regime though its' quantitative results are not reliable due to uncontrolled errors. The situation is similar with the problem of structureless polaron, where analytic solutions are known only in the weak and strong coupling regimes. Besides, reliable results for these regimes are available only for ground state properties.

Although several novel methods, capable of obtaining properties of excited states, were developed recently, variational coherent-states expansion [69] and free propagator momentum average summation [70] as a few examples, all of them, to provide reliable data in a specific regime, need either comparison with exact sum rules [71, 72] or with exact numerical results.

Application of variational methods to study of excitations is a tricky issue since, strictly speaking, they are valid only for the ground state. As an example for the importance of sum rules in variational treatment, we refer to the problem of the optical conductivity of the Fröhlich polaron. Possibility of existence of Relaxed Excited State (RES), which is a metastable state where lattice deformation has adjusted to the electronic excitation rendering stability and narrow linewidth of the spectroscopic response, was briefly mentioned by S. I. Pekar in early 50's. Then, conception of RES was rigorously formulated by J. T. Devreese with coworkers and has been a subject of extensive investigations for years [5, 73, 74, 75, 76, 77, 48, 57]. Calculations of impedance [75] in the framework of technique [78] supported the existence of a narrow stable peak in the optical conductivity. However, even the authors of [75] were skeptical about the fact that the width of RES in the strong coupling regime appeared to be more narrow than the phonon frequency, i.e. inverse time which is, according to the Heisenberg uncertainty principle, is required for the lattice readaptation. In consequent paper [77] they realized the importance of many-phonon processes and studied two-phonon contribution to optical conductivity. Importance of many phonon processes was confirmed when variational results [75] were compared with exact DMC simulations [48]. Variational result well reproduced the position of the peak in exact data though failed in description of the peak width in the strong coupling regime [48]. Finally, when approach [75] was modified and several sum rules were accurately introduced into variational model [57], both position

and width of the peak were quantitatively reproduced. Studies [57] (see Sect. 3.1), do not address rather philosophical question whether RES exists or not, though inevitably prove that, in contrast to the foregoing beliefs, there is no stable excited state of the Fröhlich polaron in the strong coupling regime. Note that sometimes excited states can not be handled by analytic methods even for weak couplings: perturbation theory expression for LF of the Fröhlich polaron model diverges at the phonon energy ω_{ph} [See (34) in Sect. 3.1.] and more elaborate treatment is necessary.

Difficulties of semianalytic methods enhance in the intermediate coupling regime where results are sometimes wrong even for ground state properties. For example, the variational approach [79], which has been considered as an intermediate coupling theory, appeared to be valid only in the weak coupling limit [45]. Special interest to the methods, giving reliable information on excited states, is triggered by the self-trapping phenomenon which occurs just in the intermediate coupling regime. This phenomenon is a dramatic transformation of QP properties when system parameters are slightly changed [3, 7, 9, 80]. In the intermediate coupling regime “trapped” QP state with strong lattice deformation around it and “free” state with weakly perturbed lattice may hybridize and resonate because of close energies at some critical value of electron-lattice interaction γ_c . It is clear that, to study self-trapping, one has to apply a method giving reliable information on excited states in the intermediate coupling regime.

2 Diagrammatic Monte Carlo and Stochastic Optimization Methods

In this section we introduce definitions of exciton-polaron properties which can be evaluated by DMC and SO methods. An idea of DMC approach for numerically exact calculation of Green functions (GFs) in imaginary times is presented in Sect. 2.1, and a short description of SO method, which is capable of making unbiased analytic continuation from imaginary times to real frequencies, is given in Sect. 2.2. Using combination of DMC and SO, one can often circumvent difficulties of analytic and traditional numerical methods. Therefore, a brief comparative analysis of advantages and drawbacks of DMC-SO machinery is given in Sect. 2.3.

To obtain information on QPs it is necessary to calculate Matsubara GF in imaginary time representation and make analytic continuation to the real frequencies [60]. For the two-particle problem (1)-(4) the relevant quantity is the two-particle GF [46, 47]

$$G_{\mathbf{k}}^{\text{pp}'}(\tau) = \langle \text{vac} | a_{\mathbf{k}+\mathbf{p}'}(\tau) h_{\mathbf{k}-\mathbf{p}'}(\tau) h_{\mathbf{k}-\mathbf{p}}^\dagger a_{\mathbf{k}+\mathbf{p}}^\dagger | \text{vac} \rangle . \quad (10)$$

(Here $h_{\mathbf{k}-\mathbf{p}}(\tau) = e^{\hat{H}\tau} h_{\mathbf{k}-\mathbf{p}} e^{-\hat{H}\tau}$, $\tau > 0$.) In the case of exciton-polaron, vacuum state $|\text{vac}\rangle$ is the state with filled valence and empty conduction bands.

For the bipolaron problem it is a system without particles. In the simpler case of a QP with two-level internal structure described by (4)-(6) the relevant quantity is the one-particle matrix GF [52, 47]

$$G_{\mathbf{k},ij}(\tau) = \langle \text{vac} | a_{i,\mathbf{k}}(\tau) a_{j,\mathbf{k}}^\dagger | \text{vac} \rangle, \quad i, j = 1, 2. \quad (11)$$

For a structureless polaron the matrix (11) reduces to one-particle scalar GF

$$G_{\mathbf{k}}(\tau) = \langle \text{vac} | a_{\mathbf{k}}(\tau) a_{\mathbf{k}}^\dagger | \text{vac} \rangle. \quad (12)$$

Information on the response to an external weak perturbation (e.g. optical absorption) is contained in the current-current correlation function $\langle J_\beta(\tau) J_\delta \rangle$ (β/δ are Cartesian indexes).

Lehmann spectral representation of $G_{\mathbf{k}}(\tau)$ [60, 61] at zero temperature

$$G_{\mathbf{k}}(\tau) = \int_0^\infty d\omega L_{\mathbf{k}}(\omega) e^{-\omega\tau}, \quad (13)$$

with the Lehmann function (LF) $L_{\mathbf{k}}(\omega)$ given in (7), reveals information on the ground and excited states. Here $\{|\nu\rangle\}$ is a complete set of eigenstates of Hamiltonian \hat{H} in a sector of given momentum \mathbf{k} : $H|\nu(\mathbf{k})\rangle = E_\nu(\mathbf{k})|\nu(\mathbf{k})\rangle$. The LF $L_{\mathbf{k}}(\omega)$ has poles (sharp peaks) on the energies of stable (metastable) states of particle. For example, if there is a stable state at energy $E(\mathbf{k})$, the LF reads $L_{\mathbf{k}}(\omega) = Z^{(\mathbf{k})} \delta(\omega - E(\mathbf{k})) + \dots$, and the state with the lowest energy $E_{\text{g.s.}}(\mathbf{k})$ in a sector of a given momentum \mathbf{k} is highlighted by asymptotic behavior of GF

$$G_{\mathbf{k}}(\tau \gg \max[\omega_{\mathbf{q},\kappa}^{-1}]) \rightarrow Z^{(\mathbf{k})} \exp[-E_{\text{g.s.}}(\mathbf{k})\tau], \quad (14)$$

where $Z^{(\mathbf{k})}$ -factor is the weight of the state. Analyzing the asymptotic behavior of similar n -phonon GFs [45, 52]

$$\langle \text{vac} | b_{\mathbf{q}_n}(\tau) \cdots b_{\mathbf{q}_1}(\tau) a_{\mathbf{p}}(\tau) a_{\mathbf{p}}^\dagger b_{\mathbf{q}_1}^\dagger \cdots b_{\mathbf{q}_n}^\dagger | \text{vac} \rangle, \quad \mathbf{p} = \mathbf{k} - \sum_{j=1}^n \mathbf{q}_j. \quad (15)$$

one obtains detailed information about lowest state. For example, important characteristics of the lowest state wave function

$$\Psi_{\text{g.s.}}(\mathbf{k}) = \sum_{i=1}^T \sum_{n=0}^{\infty} \sum_{\mathbf{q}_1 \dots \mathbf{q}_n} \theta_i(\mathbf{k}; \mathbf{q}_1, \dots, \mathbf{q}_n) c_{i,\mathbf{k}-\mathbf{q}_1 \dots -\mathbf{q}_n}^\dagger b_{\mathbf{q}_1}^\dagger \dots b_{\mathbf{q}_n}^\dagger | \text{vac} \rangle \quad (16)$$

are partial n -phonon contribution

$$Z^{(\mathbf{k})}(n) \equiv \sum_{i=1}^T \sum_{\mathbf{q}_1 \dots \mathbf{q}_n} |\theta_i(\mathbf{k}; \mathbf{q}_1, \dots, \mathbf{q}_n)|^2 \quad (17)$$

which is normalized to unity $\sum_{n=0}^{\infty} Z^{(\mathbf{k})}(n) \equiv 1$, and the average number of phonons

$$\langle N \rangle \equiv \langle \Psi_{g.s.}(\mathbf{k}) | \sum_{\mathbf{q}} b_{\mathbf{q}}^{\dagger} b_{\mathbf{q}} | \Psi_{g.s.}(\mathbf{k}) \rangle = \sum_{n=1}^{\infty} n Z^{(\mathbf{k})}(n) \quad (18)$$

in polaronic cloud. Another example is the wave function of relative electron-hole motion of exciton in the lowest state in the sector of given momentum

$$\Psi_{g.s.}(\mathbf{k}) = \sum_{\mathbf{p}} \xi_{\mathbf{k} \mathbf{p}}(g.s.) a_{\mathbf{k}+\mathbf{p}}^{\dagger} h_{\mathbf{k}-\mathbf{p}}^{\dagger} | \text{vac} \rangle . \quad (19)$$

The amplitudes $\xi_{\mathbf{k} \mathbf{p}}(g.s.)$ of this wave function can be obtained [46] from asymptotic behavior of the following GF (10)

$$G_{\mathbf{k}}^{\mathbf{p}=\mathbf{p}'}(\tau \rightarrow \infty) = |\xi_{\mathbf{k} \mathbf{p}}(g.s.)|^2 e^{-E_{g.s.}(\mathbf{k})\tau} . \quad (20)$$

Information on the excited states is obtained by the analytic continuation of imaginary time GF to real frequencies which requires to solve the Fredholm equation $G_{\mathbf{k}}(\tau) = \hat{\mathcal{F}}[L_{\mathbf{k}}(\omega)]$ (13)

$$L_{\mathbf{k}}(\omega) = \hat{\mathcal{F}}_{\omega}^{-1}[G_{\mathbf{k}}(\tau)] . \quad (21)$$

The equation (13) is a rather general relation between imaginary time GF/correlator and spectral properties of the system. For example, the absorption coefficient of light by excitons $\mathcal{I}(\omega)$ is obtained as solution of the same equation [46]

$$\mathcal{I}(\omega) = \hat{\mathcal{F}}_{\omega}^{-1} \left[\sum_{\mathbf{p}\mathbf{p}'} G_{\mathbf{k}=0}^{\mathbf{p}\mathbf{p}'}(\tau) \right] . \quad (22)$$

Besides, the real part of the optical conductivity $\sigma_{\beta\delta}(\omega)$ is expressed [48] in terms of current-current correlation function $\langle J_{\beta}(\tau) J_{\delta} \rangle$ by relation

$$\sigma_{\beta\delta}(\omega) = \pi \hat{\mathcal{F}}_{\omega}^{-1} [\langle J_{\beta}(\tau) J_{\delta} \rangle] / \omega . \quad (23)$$

2.1 Diagrammatic Monte Carlo Method

DMC Method is an algorithm which calculates GF (10)-(12) without any systematic errors. This algorithm is described below for the simplest case of structureless polaron [45], and generalizations to more complex cases can be found in consequent references⁴. DMC is based on the Feynman expansion of the Matsubara GF in imaginary time in the interaction representation

⁴ Generalization of described below technique to the case of exciton (1-2) is given in [46] and its modification for pseudo-Jahn-Teller polaron (4-6) is developed in [52, 47]. Method for evaluation of current-current correlation function can be found in [48] and a case of a polaron interacting with two kinds of bosonic fields is considered in [49].

$$G_{\mathbf{k}}(\tau) = \left\langle \text{vac} \left| T_{\tau} \left[a_{\mathbf{k}}(\tau) a_{\mathbf{k}}^{\dagger}(0) \exp \left\{ - \int_0^{\infty} \hat{H}_{\text{int}}(\tau') d\tau' \right\} \right] \right| \text{vac} \right\rangle_{\text{con}} ; \tau > 0 . \quad (24)$$

Here T_{τ} is the imaginary time ordering operator, $|\text{vac}\rangle$ is a vacuum state without particle and phonons, \hat{H}_{int} is the interaction Hamiltonian in (9). Symbol of exponent denotes Taylor expansion which results in multiple integration over internal variables $\{\tau'_1, \tau'_2, \dots\}$. Operators are in the interaction representation $\hat{A}(\tau) = \exp[\tau(\hat{H}_{\text{par}} + \hat{H}_{\text{ph}})]\hat{A}\exp[-\tau(\hat{H}_{\text{par}} + \hat{H}_{\text{ph}})]$. Index “con” means that expansion contains only connected terms where no one integral over internal time variables $\{\tau'_1, \tau'_2, \dots\}$ can be factorized.

Vick theorem expresses matrix element of time-ordered operators as a sum of terms, each is a factor of matrix elements of pairs of operators, and expansion (24) becomes an infinite series of integrals with an ever increasing number of integration variables

$$G_{\mathbf{k}}(\tau) = \sum_{m=0,2,4,\dots}^{\infty} \sum_{\xi_m} \int dx'_1 \dots dx'_m \mathcal{D}_m^{(\xi_m)}(\tau; \{x'_1, \dots, x'_m\}) . \quad (25)$$

Here index ξ_m stands for different Feynman diagrams (FDs) of the same order m . Term with $m = 0$ is the GF of the noninteracting QP $G_{\mathbf{k}}^{(0)}(\tau)$. Function $\mathcal{D}_m^{(\xi_m)}(\tau; \{x'_1, \dots, x'_m\})$ of any order m can be expressed as a factor of GFs of noninteracting quasiparticle, GFs of phonons, and interaction vortexes $V(\mathbf{k}, \mathbf{q})$. For the simplest case of Hamiltonian system expressions for GFs of QP $G_{\mathbf{k}}^{(0)}(\tau_2 - \tau_1) = \exp[-\epsilon(\mathbf{k})(\tau_2 - \tau_1)]$ ($\tau_2 > \tau_1$) and phonons $D_{\mathbf{q}}^{(0)}(\tau_2 - \tau_1) = \exp[-\omega_{\mathbf{q}}(\tau_2 - \tau_1)]$ ($\tau_2 > \tau_1$) are well known.

An important feature of the DMC method, which is distinct from the row of other exact numerical approaches, is the explicit possibility to include renormalized GFs into exact expansion without any change of the algorithm. For example, if a damping of QP, caused by some interactions not included in the Hamiltonian, is known, i.e. retarded self-energy of QP $\Sigma_{\text{ret}}(\mathbf{k}, \omega)$ is available, renormalized GF

$$\tilde{G}_{\mathbf{k}}^{(0)}(\tau) = \frac{1}{\pi} \int_{-\infty}^{\infty} d\omega e^{-\omega\tau} \frac{Im\Sigma_{\text{ret}}(\mathbf{k}, \omega)}{[\omega - \epsilon(\mathbf{k}) - Re\Sigma_{\text{ret}}(\mathbf{k}, \omega)]^2 + [Im\Sigma_{\text{ret}}(\mathbf{k}, \omega)]^2} \quad (26)$$

can be introduced instead of bare GF $G_{\mathbf{k}}^{(0)}(\tau)$. Explicit rules for evaluation of $\mathcal{D}_m^{(\xi_m)}$ do not depend on the order and topology of FD. GFs of noninteracting QPs $G_{\mathbf{k}}^{(0)}(\tau_2 - \tau_1)$ (or $\tilde{G}_{\mathbf{k}}^{(0)}(\tau_2 - \tau_1)$) with corresponding times and momenta are ascribed to horizontal lines and noninteracting GFs of phonon $D_{\mathbf{q}}^{(0)}(\tau_2 - \tau_1)$ (multiplied by the factor of corresponding vortexes $V(\mathbf{k}', \mathbf{q})V^*(\mathbf{k}'', \mathbf{q})$) are attributed to phonon propagator arch (see Fig. 1a). Then, $\mathcal{D}_m^{(\xi_m)}$ is the factor of all GSs. For example, expression for the weight of the second order term (Fig. 1b) is the following

$$\mathcal{D}_2(\tau; \{\tau'_2, \tau'_1, \mathbf{q}\}) = |V(\mathbf{k}, \mathbf{q})|^2 D_{\mathbf{q}}^{(0)}(\tau'_2 - \tau'_1) G_{\mathbf{k}}^{(0)}(\tau'_1) G_{\mathbf{k}-\mathbf{q}}^{(0)}(\tau'_2 - \tau'_1) G_{\mathbf{k}}^{(0)}(\tau - \tau'_2). \quad (27)$$

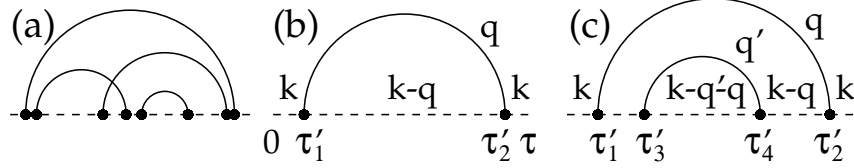


Fig. 1. (a) Typical FD contributing into expansion (25). (b) FD of the second order and (c) fourth order.

The DMC process is a numerical procedure which, basing on the Metropolis principle [81, 82], samples different FDs in the parameter space $(\tau, m, \xi_m, \{x'_m\})$ and collects statistics of external variable τ in a way that the result of this statistics converges to exact GF $G_{\mathbf{k}}(\tau)$. Although sampling of the internal parameters of one term in (25) and switch between different orders is performed within the the framework of one and the same numerical process, it is instructive to start with the procedure of evaluation of a specific term $\mathcal{D}_m^{(\xi_m)}(\tau; \{x'_1, \dots, x'_m\})$.

Starting from a set $\{\tau; \{x'_1, \dots, x'_m\}\}$, an update $x_l^{(old)} \rightarrow x_l^{(new)}$ of an arbitrary chosen parameter is suggested. This update is accepted or rejected according to Metropolis principle. After many steps, altering all variables, statistics of external variable converges to exact dependence of the term on τ . Suggestion for new value of parameter $x_l^{(new)} = \hat{S}^{-1}(R)$ is generated by random number $R \in [0, 1]$ with a normalized distribution function $W(x_l)$ in a range $x_l^{(min)} < x_l < x_l^{(max)}$. There are only two restrictions for this otherwise arbitrary function. First, new parameters $x_l^{(new)}$ must not violate FD topology, i.e., for example, internal time τ'_1 in Fig. 1c must be in the range $[x^{(min)} = 0, x^{(max)} = \tau'_3]$. Second, the distribution must be nonzero for the whole, allowed by FD topology, domain. This ergodicity property is crucial since it is necessary to sample the whole domain for convergence to exact answer. At each step, update $x_l^{(old)} \rightarrow x_l^{(new)}$ is accepted with probability $P_{acc} = M$ (if $M < 1$) and always otherwise. The ratio M has the following form

$$M = \frac{\mathcal{D}_m^{(\xi_m)}(\tau; \{x'_1, \dots, x_l^{(new)}, \dots, x'_m\})/W(x_l^{(new)})}{\mathcal{D}_m^{(\xi_m)}(\tau; \{x'_1, \dots, x_l^{(old)}, \dots, x'_m\})/W(x_l^{(old)})}. \quad (28)$$

For uniform distribution $W = \text{const} = (x_l^{(max)} - x_l^{(min)})^{-1}$, the probability of any combination of parameters is proportional to the weight function \mathcal{D} .

However, for better convergence the distribution $W(x_l^{new})$ must be as close as possible to the actual distribution given by function $\mathcal{D}_m^{(\xi_m)}(\{\dots, x_l^{(new)}, \dots\})$.

For sampling over FDs of all orders and topologies it is enough to introduce two complimentary updates. Update \mathcal{A} transforms FD $\mathcal{D}_m^{(\xi_m)}(\tau; \{x'_1, \dots, x'_m\})$ into higher order FD $\mathcal{D}_{m+2}^{(\xi_{m+2})}(\tau; \{x'_1, \dots, x'_m; \mathbf{q}', \tau'_3, \tau'_4\})$ with extra phonon arch, connecting some time points τ'_3 and τ'_4 by phonon propagator with momentum \mathbf{q}' (Fig. 1c). Note that the ratio of weights $\mathcal{D}_{m+2}^{(\xi_{m+2})}/\mathcal{D}_m^{(\xi_m)}$ is not dimensionless. Dimensionless Metropolis ratio

$$M = \frac{p_{\mathcal{A}} \mathcal{D}_{m+2}^{(\xi_{m+2})}(\tau; \{x'_1, \dots, x'_m; \mathbf{q}', \tau', \tau''\})}{p_{\mathcal{B}} \mathcal{D}_m^{(\xi_m)}(\tau; \{x'_1, \dots, x'_m\}) W(\mathbf{q}', \tau', \tau'')} . \quad (29)$$

contains normalized probability function $W(\mathbf{q}', \tau', \tau'')$, which is used for generating of new parameters⁵. Complementary update \mathcal{B} , removing the phonon propagator, uses ratio M^{-1} [45].

Note that all updates are local, i.e. do not depend on the structure of the whole FD. Neither rules nor CPU time, needed for update, depends on the FD order. DMC method does not imply any explicit truncation of FDs order due to finite size of computer memory. Ever for strong coupling, where typical number of phonon propagators N_{ph} , contributing to result, is large, influence of finite size of memory is not essential. Really, according to Central Limit Theorem, number of phonon propagators obeys Gauss distribution centered at \bar{N}_{ph} with half width of the order of $\sqrt{\bar{N}_{ph}}$ [83]. Hence, if a memory for at least $2\bar{N}_{ph}$ propagators is reserved, diagram order hardly surpasses this limit.

2.2 Stochastic Optimization Method

The problem of inverting of integral equation (13) is an ill posed problem. Due to incomplete noisy information about GF $G_{\mathbf{k}}(\tau)$, which is known with statistic errors on a finite number of imaginary times in a finite range $[0, \tau_{\max}]$, there is infinite number of approximate solutions which reproduce GF within some range of deviations and the problem is to chose “the best one”. Another problem, which is a stumbling block for decades, is the saw tooth noise instability. It occurs when solution is obtained by a naive method, e.g. by using least-squares approach for minimizing deviation measure

$$D[\tilde{L}_{\mathbf{k}}(\omega)] = \int_0^{\tau_{\max}} |G_{\mathbf{k}}(\tau) - \tilde{G}_{\mathbf{k}}(\tau)| G_{\mathbf{k}}^{-1}(\tau) d\tau . \quad (30)$$

Here $\tilde{G}_{\mathbf{k}}(\tau)$ is obtained from approximate LF $\tilde{L}_{\mathbf{k}}(\omega)$ by applying of integral operator $\tilde{G}_{\mathbf{k}}(\tau) = \mathcal{F}[\tilde{L}_{\mathbf{k}}(\omega)]$ in (13). Saw tooth instability corrupts LF in the ranges where actual LF is smooth. Fast fluctuations of the solution $\tilde{L}_{\mathbf{k}}(\omega)$ often

⁵ The factor $p_{\mathcal{A}}/p_{\mathcal{B}}$ depends on the probability to address add/remove processes.

have much larger amplitude than the value of actual LF $L_{\mathbf{k}}(\omega)$. Standard tools for saw tooth noise suppression are based on the early 60-es idea of Fillips-Tikhonov regularization method [84, 85, 86, 87]. A nonlinear functional, which suppresses large derivatives of approximate solution $\tilde{L}_{\mathbf{k}}(\omega)$, is added to the linear deviation measure (30). Most popular variant of regularization methods is the Maximal Entropy Method [61].

However, typical LF of a QP in a boson field consists of δ -functional peaks and smooth incoherent continuum with a sharp border [45, 54]. Hence, suppression of high derivatives, as a general strategy of the regularization method, fails. Moreover, any specific implementation of the regularization method uses predefined mesh in the ω space, which could be absolutely unacceptable for the case of sharp peaks. If the actual location of a sharp peak is between predefined discrete points, the rest of spectral density can be distorted beyond recognition. Finally, regularization Maximal Entropy approach requires assumption of Gauss distribution of statistic errors in $G_{\mathbf{k}}(\tau)$, which might be invalid in some cases [61].

Recently, a Stochastic Optimization (SO) method, which circumvents abovementioned difficulties, was developed [45]. The idea of the SO method is to generate a large enough number M of statistically independent nonregularized solutions $\{\tilde{L}_{\mathbf{k}}^{(s)}(\omega)\}$, $s = 1, \dots, M$, which deviation measures $D^{(s)}$ are smaller than some upper limit D_u , depending of the statistic noise of the GF $G_{\mathbf{k}}(\tau)$. Then, using linearity of expressions (13), (30), the final solution is found as the average of particular solutions $\{\tilde{L}_{\mathbf{k}}^{(s)}(\omega)\}$

$$L_{\mathbf{k}}(\omega) = M^{-1} \sum_{s=1}^M \tilde{L}_{\mathbf{k}}^{(s)}(\omega) . \quad (31)$$

Particular solution $\tilde{L}_{\mathbf{k}}^{(s)}(\omega)$ is parameterized in terms of sum

$$\tilde{L}_{\mathbf{k}}^{(s)}(\omega) = \sum_{t=1}^K \chi_{\{P_t\}}(\omega) \quad (32)$$

of rectangles $\{P_t\} = \{h_t, w_t, c_t\}$ with height $h_t > 0$, width $w_t > 0$, and center c_t . Configuration

$$\mathcal{C} = \{\{P_t\}, t = 1, \dots, K\} , \quad (33)$$

which satisfies normalization condition $\sum_{t=1}^K h_t w_t = 1$, defines function $\tilde{G}_{\mathbf{k}}(\tau)$. The procedure of generating particular solution starts from stochastic choice of initial configuration $\mathcal{C}_s^{\text{init}}$. Then, deviation measure is optimized by a randomly chosen consequence of updates until deviation is less than D_u . In addition to updates, which do not change number of terms in the sum (32), there are updates which increase or decrease number K . Hence, since the number of elements K is not fixed, any spectral function can be reproduced with desired accuracy.

Although each particular solution $\tilde{L}_{\mathbf{k}}^{(s)}(\omega)$ suffers from saw tooth noise at the area of smooth LF, statistical independence of each solution leads to self averaging of this noise in the sum (32). Note that suppression of noise happens without suppression of high derivatives and, hence, sharp peaks and edges are not smeared out in contrast to regularization approaches. Therefore, saw tooth noise instability is defeated without corruption of sharp peaks and edges. Moreover, continuous parameterization (32) does not need predefined mesh in ω -space. Besides, since the Hilbert space of solution is sampled directly, any assumption about distribution of statistical errors is not necessary.

SO method was successfully applied to restore LF of Fröhlich polaron [45], Rashba-Pekar exciton-polaron [54], hole-polaron in t - J -model [53, 49], and many-particle spin system [88]. Calculation of the optical conductivity of polaron by SO method can be found in [48]. SO method appeared to be helpful in cases when GF's asymptotic limit, giving information about ground state, can not be reached. For example, sign fluctuations of the terms in expansion (25) for a hole in the t - J -model lead to poor statistics at large times [53], though, SO method is capable of recovering energy and Z -factor even from GF known only at small imaginary times [53].

2.3 Advantages and Drawbacks of DMC-SO Machinery

Among numerical methods, capable of obtaining quantitative results in the problem of exciton (1) and (2), one can list time-dependent density functional theory [89], Hanke-Sham technique of correcting particle-hole excitation energy [90, 91], and approaches directly solving Bethe-Salpeter equation [92, 93, 94]. The latter ones provide rather accurate information on the two-particle GF. However, usage of finite mesh in direct/reciprocal space, which is avoided in DMC method, leads to its' failure in Wannier regime [93].

In contrast to DMC method, none of the traditional numeric methods can give reliable results for measurable properties of excited states of polaron at arbitrary range of electron-phonon interaction for the macroscopic system in the thermodynamic limit. Exact diagonalization method [95, 96, 97, 98] can study excited states though only on rather small finite size systems and results of this method are not even justified in the variational sense in the thermodynamic limit [99]. There is a batch of rather effective variational "exact translation" methods [99, 100, 101, 102, 103] where basis is chosen in the momentum space and, hence, the variational principle is applied in the thermodynamic limit. Although these methods can reveal few discrete excited states, its fail for long-range interaction and for dispersive, especially acoustic phonons due to catastrophic growth of variational basis. A non perturbative theory, which is able to give information about spectral properties in the thermodynamic limit at least for one electron, is Dynamical Mean Field Theory [104, 105, 106, 107]. However it gives an exact solution only in the case of infinite dimension which does not correspond to a realistic system and can be considered only as a guide for extrapolation to finite dimensions [108].

Recently developed cluster perturbation theory, where exact diagonalization of a cluster is further improved by taking into account inter-cluster interaction [109, 110, 111, 112, 113], is applicable for study of the excited states, but limited to one-dimensional lattices or two-dimensional systems with short-range interaction. Traditional density-matrix renormalization group method [114, 115, 116, 117, 118] is very effective though mostly limited to one-dimensional systems and ladders. Finally, recently developed path integral quantum Monte Carlo algorithm [119, 120, 121, 122] is valid for any dimension and properly takes into account quasi long-range interactions [123]. Path integral method is capable of obtaining the density of states [119, 120] and isotope exponents [121, 124]. However calculations of measurable characteristics of excited states, such as ARPES or optical conductivity, by this method were never reported.

In conclusion, none of methods, except DMC-SO combination, can obtain at the moment approximation-free results for *measurable physical quantities* for a few QPs interacting with a macroscopic bosonic bath *in the thermodynamic limit*. Indeed, there are limitations of the DMC and SO methods. DMC method does not work in many-fermion systems due to sign problem and SO method fails at high temperatures, comparable to energies of dominant spectral peaks, because even very small statistical noise of GFs turns Fredholm equation (13) into essentially “ill defined” problem [84].

3 Spectral Properties of the Fröhlich Polaron

Before development of DMC-SO methods, the information on the excited states of polaron models, especially the Fröhlich one, was very limited. Knowledge of LF was based on results of infinite-dimensions approximation [125], exact diagonalization [126, 96, 97, 97], or strong coupling expansion [127]. No one of the above techniques was capable of obtaining the LF of polaron without approximations, especially for long-range interaction where difficulties of traditional numerical methods dramatically increase. In a similar way, optical conductivity (OC) of Fröhlich model was known only in strong coupling expansion approximation [128], within the framework of the perturbation theory [129], or was based on the variational Feynman path integral technique [75]. In this sect. we consider exact DMC-SO results on LF [45] and OC [48, 57] of Fröhlich polaron model.

3.1 Lehmann Function of the Fröhlich Polaron

The perturbation theory expression for the high-energy part ($\omega > 0$) of the LF for arbitrary interaction potential $V(|\mathbf{q}|)$ reads [45] (frequency of the optical phonon ω_{ph} is set to unity)

$$L_{\mathbf{k}=0}(\omega > 0) = \frac{1}{\sqrt{2\pi^2}} \frac{\sqrt{\omega-1}}{\omega^2} |V(\sqrt{2(\omega-1)})|^2 \theta(\omega-1). \quad (34)$$

Low-energy part of the LF for the short-range interaction $V(|\mathbf{q}|) =$

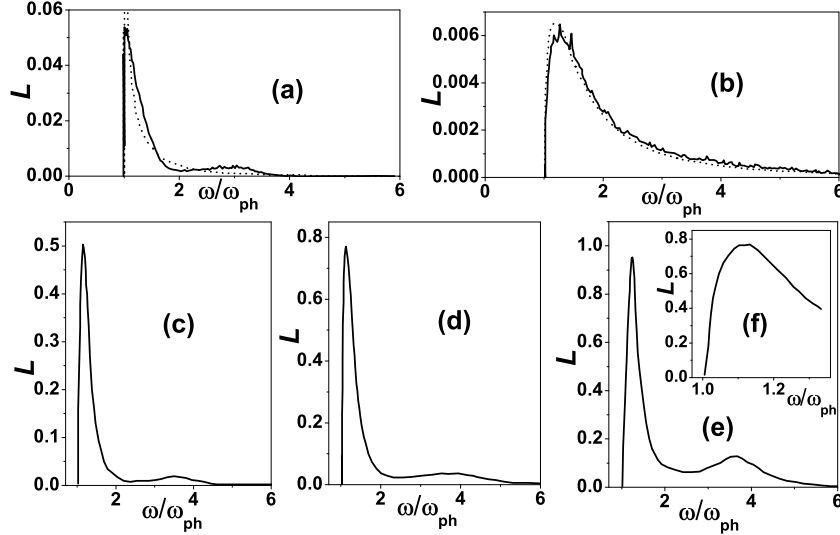


Fig. 2. Comparison of the numerical results (solid lines) and the perturbation theory (dashed lines) for the LFs of the Fröhlich model with $\alpha = 0.05$ (a) and the short-range interaction model with $\alpha = 0.05$ and $\kappa = 1$ (b). LFs of Fröhlich polaron for $\alpha = 0.5$ (c), $\alpha = 1$ (d) and $\alpha = 2$ (e). Energy is measured from that of the ground state of the polaron. The initial fragment of the LF for $\alpha = 1$ is shown in the inset (f).

$i (2\sqrt{2}\alpha\pi)^{1/2} (q^2 + \kappa^2)^{-1/2}$, reducing to the Fröhlich one when $\kappa \rightarrow 0$, is

$$L_{\mathbf{k}=0}(\omega < 0) = \frac{\alpha}{(\kappa + \sqrt{2})^2} \delta\left(\omega + \alpha \frac{\sqrt{2}}{\kappa + \sqrt{2}}\right). \quad (35)$$

Comparison of low-energy parts of the LF of the Fröhlich model, obtained by DMC-SO and taken from (35), shows perfect agreement for $\alpha = 0.05$: the accuracy for the polaron energy and Z-factor is about 10^{-4} . On the other hand, high-energy part of numeric result (Fig. 2) significantly deviates from that of the analytic expression (35). This is not surprising since for Fröhlich polaron the perturbation theory expression is diverging as $\omega \rightarrow \omega_{ph}$ and, therefore the perturbation theory breaks down. When perturbation theory is obviously valid, e.g. for the case of finite $\kappa = 1$, there is a perfect agreement between analytic expression and DMC-SO results (Fig. 2b). Note that the high-energy part of $L_{\mathbf{k}=0}(\omega)$ is successfully restored by SO method despite the fact that the total weight of the feature for $\alpha = 0.05$ is less than 10^{-2} .

The main deviation of the actual LF from the perturbation theory result is the extra broad peak in the actual LF at $\omega \sim 3.5$. To study this feature $L_{\mathbf{k}=0}(\omega)$ was calculated for $\alpha = 0.5$, $\alpha = 1$, and $\alpha = 2$ (Fig. 2c-e). The peak

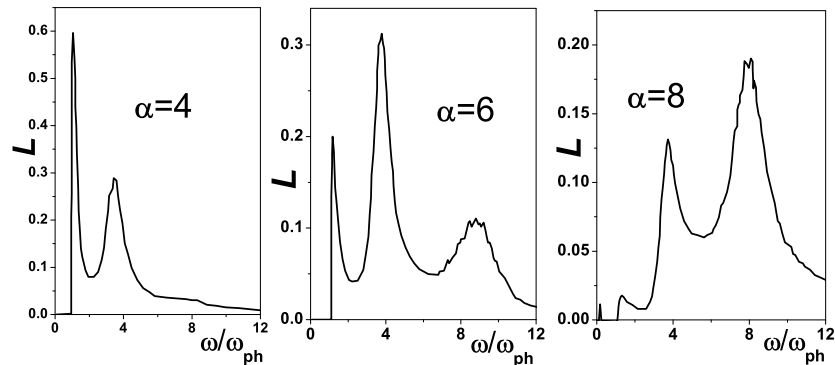


Fig. 3. Evolution of spectral density with α in the cross-over region from intermediate to strong couplings. The polaron ground state peak is shown only for $\alpha = 8$. Note that the spectral analysis still resolves it, despite its very small weight $< 10^{-3}$.

is seen for higher values of the interaction constant and its weight grows with α . Near the threshold, $\omega = 1$, LF demonstrates the square-root dependence $\sim \sqrt{\omega - 1}$ (Fig. 2f).

To trace the evolution of the peak at higher values of α the LF was calculated [45] for $\alpha = 4$, $\alpha = 6$, and $\alpha = 8$ (Fig. 3). At $\alpha = 4$ the peak at $\omega \sim 4$ already dominates. Moreover, a distinct high-energy shoulder appears at $\alpha = 4$, which transforms into a broad peak at $\omega \sim 8.5$ in the LF for $\alpha = 6$. The LF for $\alpha = 8$ demonstrates further redistribution of the spectral weight between different maxima without significant shift of the peak positions.

3.2 Optical Conductivity of the Fröhlich Polaron: Validity of the Franck-Condon Principle in the Optical Spectroscopy

The FC principle [130, 131] and its validity have been widely discussed in studies of optical transitions in atoms, molecules [132, 133], and solids [134, 9]. Generally, the FC principle means that if only one of two coupled subsystems, e.g. an electronic subsystem, is affected by an external perturbation, the second subsystem, e.g., the lattice, is not fast enough to follow the reconstruction of the electronic configuration. It is clear that the justification for the FC principle is the short characteristic time of the measurement process $\tau_{mp} \ll \tau_{ic}$, where τ_{mp} is related to the energy gap between the initial and final states, ΔE , through the uncertainty principle: $\tau_{mp} \simeq \hbar/(\Delta E)$ and τ_{ic} is the time necessary to adjust the lattice when the electronic component is perturbed. Then, the spectroscopic response considerably depends on the value of the ratio τ_{mp}/τ_{ic} . For example, in mixed valence systems, where the ionic valence fluctuates between configurations f^5 and f^6 with characteristic time $\tau_{ic} \approx 10^{-13}$ s, spectra of fast and slow experiments are dramatically different [135, 136]. Photoemission experiments with short characteristic times $\tau_{mp} \approx 10^{-16}$ s (FC regime), reveal two lines, corresponding to f^5 and f^6

states. On the other hand slow Mössbauer isomer shift measurements with $\tau_{mp} \approx 10^{-9}$ s show a single broad peak with mean frequency lying between signals from pure f^5 and f^6 shells. Finally, according to paradigm of measurement process time, magnetic neutron scattering with $\tau_{mp} \approx \tau_{ic}$ revealed both coherent lines with all subsystems dynamically adjusted and broad incoherent remnants of strongly damped excitation of f^5 and f^6 shells [137, 138]. Actually, the meaning of the times τ_{ic} and τ_{mp} varies with the system and with the measurement process.

To study the interplay between measurement process time τ_{mp} and adjustment time τ_{ic} , the OC of the Fröhlich polaron was studied in [57] from the weak to the strong coupling regime by three methods. DMC method gives numerically exact answer which is compared with memory function formalism (MFF), which is able to take dynamical lattice relaxation into account, and strong coupling expansion (SCE) which assumes FC approach. It was found that near critical coupling $\alpha_c \approx 8.5$ a dramatic change of the OC spectrum occurs: dominating peak of OC splits into two satellites. In this critical regime the upper (lower) one quickly decreases (increases) its spectral weight as the value of coupling constant increases. Besides, while OC follows prediction of MFF at $\alpha < \alpha_c$, its dependence switches to that predicted by SCE for larger couplings. It was concluded that, for the OC measurement of polaron, the adjustment time $\tau_{ic} \approx \hbar/\mathcal{D}$ is set by typical nonadiabatic energy \mathcal{D} . Nonadiabaticity destroys FC classification at $\alpha < \alpha_c$ while FC principle rapidly regains its validity at large couplings due to fast growth of energy separation between initial and final states of optical transitions.

Comparison of exact DMC-SO data for OC with existing results of approximate methods showed [48] that the Feynman path integral technique [75] of Devreese, De Sitter, and Goovaerts, where OC is calculated starting from the Feynman variational model [139], is the only successfully describing evolution of the energy of the main peak in OC with coupling constant α (see [58]). However, starting from the intermediate coupling regime this approach fails to reproduce the peak width. Subsequently, the path integral approach was rewritten in terms of MFF [140]. Then, in [57] the extended MFF formalism, which introduces dissipation processes fixed by exact sum rules, was developed [141].

As shown in Fig. 4a, in the weak coupling regime, the MFF, with or without dissipation, is in very good agreement with DMC data, showing significant improvement with respect to weak coupling perturbation approach [129] which provides a good description of OC spectra only for very small values of α . For $1 \leq \alpha \leq 8$, where standard MFF fails to reproduce peak width (Fig. 4b-d) and even the peak position (Fig. 4c), the damping, introduced to extended MFF scheme, becomes crucial. Results of extended MFF are accurate for the peak energy and quite satisfactory for the peak width (Fig. 4b-e). Note that the broadening of the peak in DMC data is not a consequence of poor quality of analytic continuation procedure since DMC-SO methods is capable of revealing such fine features as 2- and 3-phonon thresholds of emission (Fig. 4b).

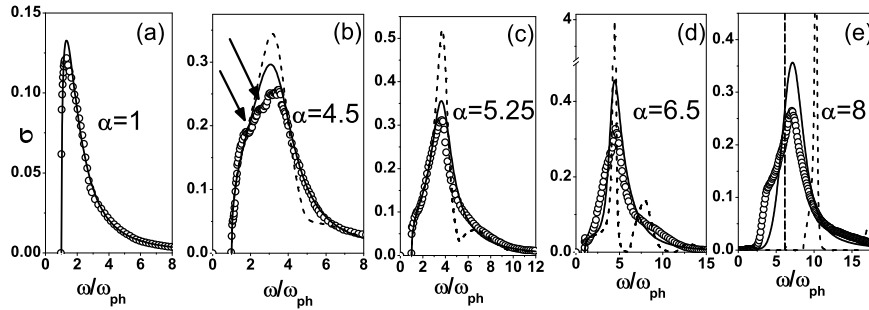


Fig. 4. Comparison of the optical conductivity calculated by DMC method (circles), extended MFF (solid line), and DSG [75, 140] (dashed line) for different values of α . The slanted arrows indicate 2- and 3-phonon thresholds of absorption.

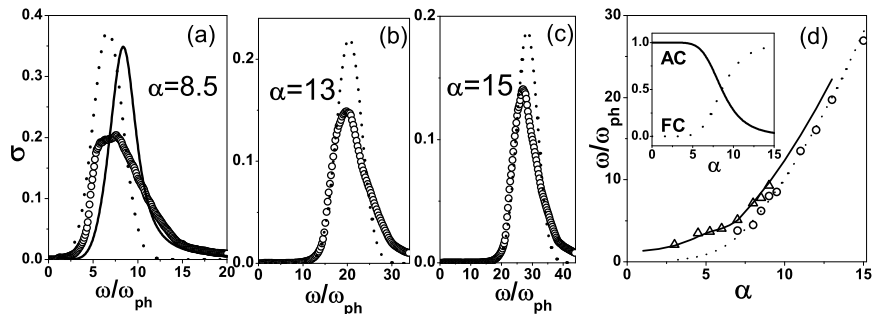


Fig. 5. (a)-(c) Comparison of the optical conductivity calculated within the DMC method (circles), the extended MFF (solid line), and SCE (dotted line) for different values of α . (d) The energy of lower- and higher-frequency features (circles and triangles, respectively) compared with the FC transition energy with the SCE (dashed line) and with the energy of the peak obtained from the extended MFF (solid line). In the inset, the weights of FC and adiabatically connected transitions are shown as a function of α (for $\eta = 1.3$).

However, a dramatic change of OC occurs around critical coupling strength $\alpha_c \approx 8.5$. The dominating peak of OC splits into two ones, the energy of lower one corresponding to the predictions of SCR expansion and that of upper one obeying extended MFF value (Fig. 5a). The shoulder, corresponding to dynamical extended MFF contribution, rapidly decreases its intensity with increase of α and at large α (Fig. 5b-c) the OC is in good agreement with strong coupling expansion, assuming FC scheme. Finally, comparing energies of the peaks, obtained by DMC, extended MFF and FC strong coupling expansion (Fig. 5d), we conclude that at critical coupling $\alpha_c \approx 8.5$ the spectral properties rapidly switch from dynamic, when lattice relaxes at transition, to FC regime, where nuclei are frozen in initial configuration.

In order to get an idea of the FC breakdown authors of [57] consider the following arguments. The approximate adiabatic states are not exact eigenstates of the system. These states are mixed by nondiagonal matrix elements of the

nonadiabatic operator \mathcal{D} and exact eigenstates are linear combinations of the adiabatic wavefunctions. Being interested in the properties of transition from ground (g) to an excited (ex) state, whose energy correspond to that of the OC peak, it is necessary to consider mixing of only these states and express exact wavefunctions as a linear combinations [142, 143] of ground and excited adiabatic states. The coefficients of superposition are determined from standard techniques [142, 143] where nondiagonal matrix elements of the nonadiabatic operator [142] are expressed in terms of matrix elements of the kinetic energy operator M , the gap between excited and ground state $\Delta E = E_{ex} - E_g$ and the number n_β of phonons in adiabatic state:

$$\mathcal{D}^\pm = M(\Delta E)^{-1} \sqrt{n_\beta + 1/2 \pm 1/2} + M^2(\Delta E)^{-2}. \quad (36)$$

The extent to which lattice can follow transition between electronic states, depends on the degree of mixing between initial and final exact eigenstates through the nonadiabatic interaction. If initial and ground states are strongly mixed, the adiabatic classification has no sense and, therefore, the FC processes have no place and lattice is adjusted to the change of electronic states during the transition. In the opposite limit adiabatic approximation is valid and FC processes dominate. The estimation for the weight of FC component I_{FC} [57] is equal to unity in the case of zero mixing and zero in the case of maximal mixing. The weight of adiabatically connected (AC) transition $I_{AC} = 1 - I_{FC}$ is defined accordingly. Non-diagonal matrix element M is proportional to the root square of α with a coefficient η of the order of unity. In the strong coupling regime, assuming that $\Delta E \approx \gamma\alpha^2$ ($\gamma \approx 0.1$ from MC data), and $n_\beta \approx \Delta E$ ($n_\beta \gg 1$), one gets

$$I_{FC} = [1 + 4(\tau_{mp}/\tau_{ic})^2]^{-1}, \quad (37)$$

where $\tau_{mp} = 1/\Delta E$ and $\tau_{ic} = 1/D$. For η of the order of unity one obtains qualitative description of a rather fast transition from AC- to FC-dominated transition, when I_{FC} and I_{AC} exchange half of their weights in the range of α from 7 to 9. The physical reason for such quick change is the faster growth of energy separation $\Delta E \sim \alpha^2$ compared to that of the matrix element $M \sim \alpha^{1/2}$. Finally, for large couplings, initial and final states become adiabatically disconnected. The rapid AC-FC switch has nothing to do with the self-trapping phenomenon where crossing and hybridization of the ground and an excited states occurs. This phenomenon is a property of transition between different states and related to the choice whether lattice can or can not follow adiabatically the change of electronic state at the transition.

4 Self-Trapping

In this section we consider the self-trapping (ST) phenomenon which, due to essential importance of many-particle interaction of QP with bosonic bath of

macroscopic system, was never addressed by exact method before. We start with a basic definition of the ST phenomenon and introduce the adopted criterion for its existence. Then, generic features of ST are demonstrated on a simple model of Rashba-Pekar exciton-polaron in Sect. 4.1. It is shown in Sect. 4.2 that the criterion is not a dogma since even in one dimensional system, where ST is forbidden by criterion of existence, one can observe all main features of ST due to peculiar nature of electronic states.

In general terms [7, 80], ST is a dramatic transformation of a QP properties when system parameters are slightly changed. The physical reason of ST is a quantum resonance, which happens at some critical interaction constant γ_c , between “trapped” (T) state of QP with strong lattice deformation around it and “free” (F) state. Naturally, ST transition is not abrupt because of nonadiabatic interaction between T and F states and all properties of the QP are analytic in γ [144]. At small $\gamma < \gamma_c$, ground state is an F state which is weakly coupled to phonons while excited states are T states and have a large lattice deformation. At critical couplings $\gamma \approx \gamma_c$ a crossover and hybridization of these states occurs. Then, for $\gamma > \gamma_c$ the roles of the states exchange. The lowest state is a T state while the upper one is an F state.

First, and up to now the only quantitative criterion for ST existence was given in terms of the ground state properties in the adiabatic approximation. This criterion considers stability of the delocalized state in undistorted lattice $\Delta = 0$ with respect to the energy gain due to lattice distortion $\Delta' \neq 0$. ST phenomenon occurs when completely delocalized state with $\Delta = 0$ is separated from distorted state with $\Delta' \neq 0$ by a barrier of adiabatic potential. One of these states is stable while another one is meta-stable. The criterion of barrier existence is defined in terms of the stability index

$$s = d - 2(1 + l), \quad (38)$$

where d is the system dimensionality. Index l determines the range of the force $\lim_{q \rightarrow 0} \psi(q) \sim q^{-l}$, where $\psi(\mathbf{R})$ is the kernel of interaction $U(\mathbf{R}_n) = \psi(\mathbf{R}_n - \mathbf{R}_{n'})\nu(\mathbf{R}_{n'})$ connecting potential $U(\mathbf{R}_n)$ with generalized lattice distortion $\nu(\mathbf{R}_{n'})$ [7]. The barrier exists for $s > 0$ and does not exist for $s < 0$. The discontinuous change of the polaron state, i.e. ST, occurs in the former case while does not happen in the latter case. When $s = 0$, this scaling argument alone can not conclude the presence or absence of the ST and more detailed discussion for each model is needed.

4.1 Typical Example of the Self-Trapping: Rasba-Pekar Exciton-Polaron

Classical example of a system with ST phenomenon is the three dimensional continuous Rasba-Pekar exciton-polaron in the approximation of intraband scattering, i.e. when polar electron-phonon interaction (EPI) with dispersionless optical phonons $\omega_{\text{ph}} = 1$ does not change the wave function of internal

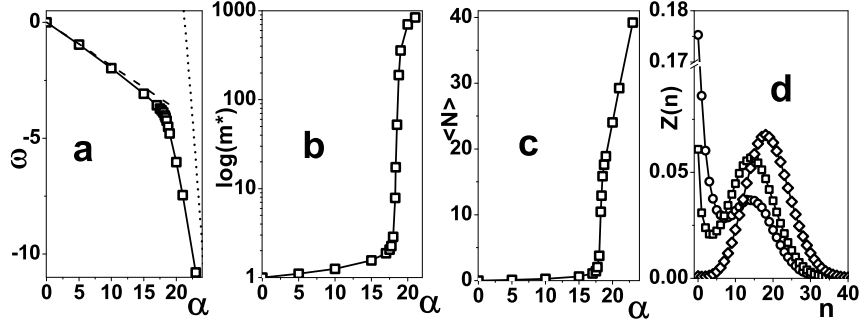


Fig. 6. The ground-state energy (a), effective mass (b), and average number of phonons as function of coupling constant (c). Partial weights of n -phonon states (d) in the polaron ground state ($\mathbf{k} = 0$) at $\gamma = 18$ (circles), $\gamma = 18.35$ (squares), and $\gamma = 19$ (diamonds). Dotted line in panel (a) is the result of strong coupling limit and dashed line is the result of perturbation theory.

electron-hole motion. System is defined as a structureless QP with dispersion $\epsilon(\mathbf{k}) = k^2/2$ and short range coupling to phonons [54, 7]. General criterion of the existence of ST is satisfied for three dimensional system with short range interaction [54, 7, 50] and, thus, one expects to observe typical features of the phenomenon.

It is shown [54] that in the vicinity of the critical coupling $\gamma_c \approx 18$ the average number of phonons $\langle N \rangle$ in (18) and effective mass m^* quickly increase in the ground state by several orders of magnitude (Fig. 6b-c). Besides, a quantum resonance between polaronic phonon clouds of F and T state is demonstrated. Distribution of partial n -phonon contributions $Z^{(\mathbf{k}=0)}(n)$ in (17) has one maximum at $n = 0$ in the weak coupling regime, which corresponds to weak deformation, and one maximum at $n \gg 1$ in the strong coupling regime, which is the consequence of a strong lattice distortion. However, due to F-T resonance there are two distinct peaks at $n = 0$ and $n \gg 1$ for $\gamma \approx \gamma_c$ (Fig. 6d).

Near the critical coupling γ_c the LF of polaron has several stable states (Fig. 7 a-b) below the threshold of incoherent continuum $E_{\text{gs}} + \omega_{\text{ph}}$. Any state above the threshold is unstable because emission of a phonon with transition to the ground state at $\mathbf{k} = 0$ with energy E_{gs} is allowed. On the other hand, decay is forbidden by conservation laws for states below the threshold. Dependence of the energies of ground and excited resonances on the interaction constant resembles a picture of crossing of several states interacting with each other (Fig. 7c).

According to the general picture of the ST phenomenon, lowest F state in the weak coupling regime at $\mathbf{k} = 0$ has small effective mass $m^* \approx m$ of the order of the bare QP mass m . To the contrary, the effective mass of excited state $m^* \gg m$ is large. Hence, below the critical coupling the energy of the F state, which is lowest at $\mathbf{k} = 0$, has to reach a flat band of T state at some momentum. Then, F and T state have to hybridize and exchange in

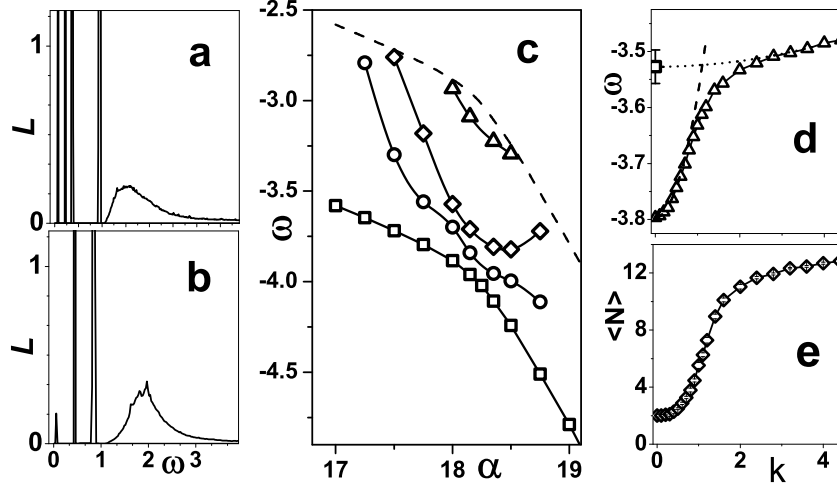


Fig. 7. LF $L_{(\mathbf{k}=0)}(\omega)$ at critical coupling $\gamma = \gamma_c$ (a) and for $\gamma > \gamma_c$ (b). Energy is counted from the polaron ground state. (c) Dependence of energy of ground state (squares) and stable excited states (circles, diamonds, and triangles) on the coupling constant. Dashed line is the threshold of the incoherent continuum. Dependence of energy (d) and average number of phonons (e) on the wave vector at $\gamma < \gamma_c$ (circles and rectangles). Dashed line is the effective mass approximation $E^{(\mathbf{k})} = E_{gs} + \mathbf{k}^2/2m^*$ for parameters $E_{gs} = -3.7946$ and $m^* = 2.258$, obtained by DMC estimators for given value of γ . Dotted line is a parabolic dispersion law which is fitted to last 4 points of energy dispersion curve with parameters $E_1 = -3.5273$ and $m_1^* = 195$. Empty square is the energy of first excited stable state at zero momentum obtained by SO method.

energy. DMC data visualize this picture (Fig. 7 d-e). After F state crosses the flat band of excited T state, the average number of phonons increases and dispersion becomes flat.

It is natural to assume that above the critical coupling the situation is opposite: ground state is the T state with large effective mass while excited F state has small, nearly bare, effective mass. Indeed, this assumption was confirmed in the framework of another model which is considered in Sect. 6.1. Moreover, it was shown that in the strong coupling regime excited resonance inherits not only bare effective mass around $\mathbf{k} = 0$ but the whole dispersion law of the bare QP [49].

4.2 Degeneracy Driven Self-Trapping

According to the criterion (38), ST phenomenon in one-dimensional system does not occur. Although this statement is probably valid for the case of single band in relevant energy range, it is not the case for the generic multi-band cases. This fact has been unnoticed for many years,

which prevented the proper explanation of puzzling physics of quasi-one-dimensional compound Anthracene-PMDA, although its optical properties [65, 145, 146, 147, 66, 148] directly suggested resonance of T and F states. The reason is that in Anthracene-PMDA, in contrast to conditions at which criterion (38) is obtained, there are two, nearly degenerate exciton bands. Then, one can consider quasi-degenerate self-trapping mechanism when ST phenomenon is driven by nondiagonal interaction of phonons with quasidegenerate exciton levels [52]. Such mechanism was already suggested for explanation of properties of mixed valence systems [143] though its relevance was never proved by an exact approach.

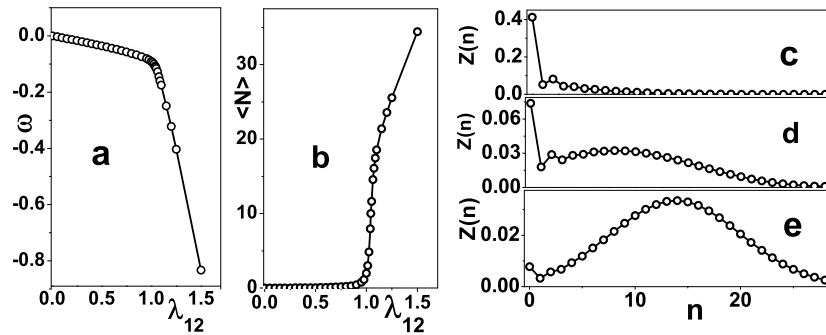


Fig. 8. Dependence of energy (a) and average number of phonons (b) on the non-diagonal coupling constant λ_{12} at $\lambda_{11} = 0$ and $\lambda_{22} = 0.25$. Phonon distributions in polaron cloud below ST point at $\lambda_{12} = 1.0125$ (c), at ST point at $\lambda_{12} = 1.0435$ (d), and above ST coupling at $\lambda_{12} = 1.0625$ (e).

The minimal model to demonstrate the mechanism of quasi-degenerate self-trapping involves one optical phonon branch with frequency $\omega_{ph} = 0.1$ and two exciton branches with energies $\epsilon_{1,2}(q) = \Delta_{1,2} + 2[1 - \cos(q)]$, where $\Delta_1 = 0$ and $\Delta_2 = 1$. Presence of short range diagonal γ_{22} and nondiagonal γ_{12} interactions (with corresponding dimensionless constants $\lambda_{22} = \gamma_{22}^2/(2\omega)$ and $\lambda_{12} = \gamma_{12}^2/(2\omega)$) leads to classical self-trapping behavior even in one-dimensional system [52] (see Fig. 8).

5 Exciton

Despite numerous efforts over the years, there has been no rigorous technique to solve for exciton properties even for the simplest model (1)-(2) which treats electron-electron interactions as a static renormalized Coulomb potential with averaged dynamical screening. The only solvable cases are the Frenkel small-radius limit [67] and the Wannier large-radius limit [68] which describe molecular crystals and wide gap insulators with large dielectric constant, respectively. Meanwhile, even the accurate data for the limits of validity of the

Wannier and Frenkel approximations have not been available. As discussed in Sects. 1.2 and 2.3, semianalytic approaches has little to add to problem when quantitative results are needed whereas traditional numerical methods fail to reproduce them even in the Wannier regime. To the contrary, DMC results do not contain any approximation.

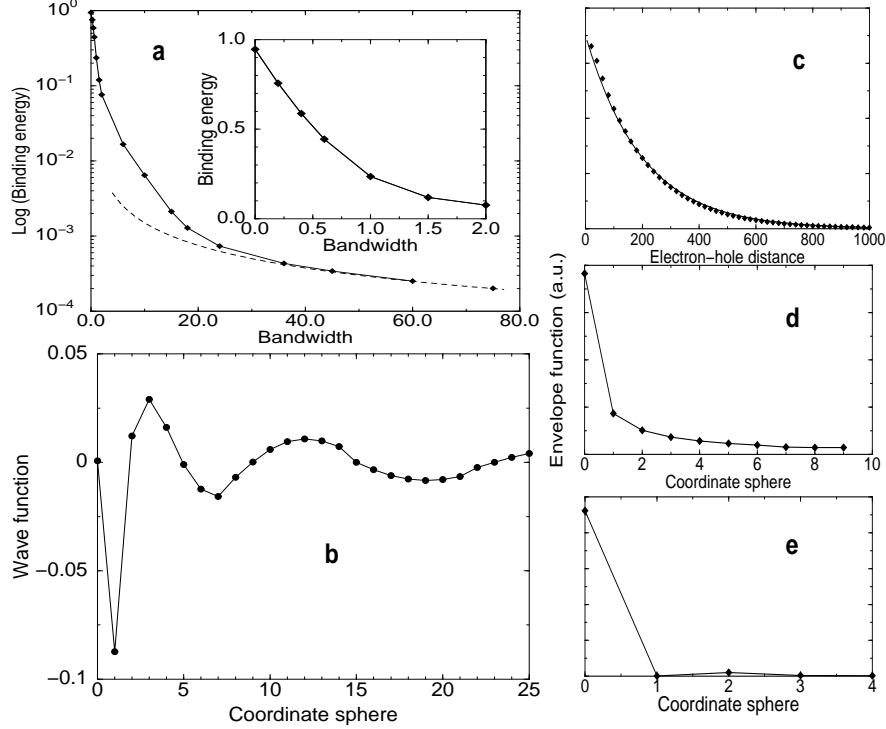


Fig. 9. Panel (a): dependence of the exciton binding energy on the bandwidth $E_c = E_v$ for conduction and valence bands. The dashed line corresponds to the Wannier model. The solid line is the cubic spline, the derivatives at the right and left ends being fixed by the Wannier limit and perturbation theory, respectively. Inset in panel (a): the initial part of the plot. Panel (b): the wave function of internal motion in real space for the optically forbidden monopolar exciton. Panels (c)-(e): the wave function of internal motion in real space: (c) Wannier [$E_c = E_v = 60$]; (d) intermediate [$E_c = E_v = 10$]; (e) near-Frenkel [$E_c = E_v = 0.4$] regimes. The solid line in the panel (c) is the Wannier model result while solid lines in other panels are to guide the eyes only.

To study conditions of validity of limiting regimes by DMC method, electron-hole spectrum of three dimensional system was chosen in the form of symmetric valence and conduction bands with width E_c and direct gap E_g

at zero momentum [46]. For large ratio $W = E_c/E_g$, when $W > 30$, exciton binding energy is in good agreement with Wannier approximation results (Fig. 9a) and probability density of relative electron-hole motion corresponds (Fig. 9c) to hydrogen-like result. The striking result is the requirement of rather large valence and conduction bandwidths ($W > 20$) for applicability of Wannier approximation. For smaller values of W the binding energy and wave function of relative motion (Fig. 9d) deviate from large radius results. In the similar way, conditions of validity of Frenkel approach are rather restricted too. Moreover, even strong localization of wave function does not guarantee good agreement between exact and Frenkel approximation result for binding energy. At $1 < W < 10$ the wave function is already strongly localized though binding energy considerably differs from Frenkel approximation result. For example, at $W = 0.4$ relative motion is well localized (Fig. 9e) whereas the binding energy of Frenkel approximation is two times larger than exact result (Inset in Fig. 9a).

A study of conditions necessary for formation of charge transfer exciton in three dimensional systems is crucial to finalize protracted discussion of numerous models concerning properties of mixed valence semiconductors [149]. A decade ago unusual properties of SmS and SmB₆ were explained by invoking the excitonic instability mechanism assuming charge-transfer nature of the optically forbidden exciton [150, 151]. Although this model explained quantitatively the phonon spectra [152, 153], optical properties [154, 155], and magnetic neutron scattering data [138], it's basic assumption has been criticized as being groundless [156, 157]. To study excitonic wavefunction, dispersions of valence and conduction bands were chosen as it is typical for mixed valence materials: almost flat valence band is separated from broad conduction band, having maximum in the centre and minimum at the border of Brillouin zone [46]. Results presented in Fig. 9b support assumption of [150, 151] since wave function of relative motion has almost zero on-site component and maximal charge density at near neighbors.

6 Polarons in Undoped High Temperature Superconductors

It is now well established that the physics of high temperature superconductors is that of hole doping a Mott insulator [158, 159, 160]. Even a single hole in a Mott insulator, i.e. a hole in an antiferromagnet in case of infinite Hubbard repulsion U , is substantially influenced by many-body effects [10] because it's jump to a neighboring site disturbs antiferromagnetic arrangement of spins. Hence a thorough understanding of the dynamics of doped holes in Mott insulators has attracted a great deal of recent interest. The two major interactions relevant to the electrons in solids are electron-electron interactions (EEL) and electron-phonon interactions (EPI). The importance of the former at low doping is no doubt essential since the Mott insulator is driven

by strong Hubbard repulsion, while the latter was considered to be largely irrelevant to superconductivity based on the observations of a small isotope effect on the optimal T_c [161] and an absence of a phonon contribution to the resistivity (for review see [162]).

On the other hand, there are now accumulating evidences that the EPI plays an important role in the physics of cuprates such as (i) an isotope effect on superfluid density ρ_s and T_c away from optimal doping [163], (ii) neutron and Raman scattering [164, 165, 166] experiments showing strong phonon softening with both temperature and hole doping, indicating that EPI is strong [167, 168]. Furthermore, the recent studies of cuprates by the angle resolved photoemission spectroscopy (ARPES), which spectra are proportional to the LF (7) [32], resulted in the discovery of the dispersion "kinks" at around 40-70meV measured from the Fermi energy, in the correct range of the relevant oxygen related phonons [169, 170, 171]. These particular phonons - oxygen buckling and half-breathing modes are known to soften with doping [172, 164] and with temperature [170, 171, 172, 164, 165, 166] indicating strong coupling. The quick change of the velocity can be predicted by any interaction of a quasiparticle with a bosonic mode, either with a phonon [170, 171] or with a collective magnetic resonance mode [173, 174, 175]. However, the recently discovered "universality" of the kink energy for LSCO over the entire doping range [176] casts doubts on the validity of the latter scenario as the energy scale of the magnetic excitation changes strongly with doping.

Besides, measured in undoped high T_c materials ARPES revealed apparent contradiction between momentum dependence of the energy and linewidth of the QP peak. On the one hand the experimental energy dispersion of the broad peak in many underdoped compounds [31, 177] obeys the theoretical predictions [178, 179], whereas the experimental peak width is comparable with the bandwidth and orders of magnitude larger than that obtained from theory of Mott insulator [53]. Early attempts to interpret this anomalously short lifetime of a hole by an interaction with additional nonmagnetic bosonic excitations, e.g. phonons [180], faced generic question: is it possible that interaction with media leaves the energy dispersion absolutely unrenormalized, while, induces a decay which inverse life-time is comparable or even larger than the QP energy dispersion? A possibility of an extrinsic origin of this width can be ruled out since the doping induces further disorder, while a sharper peak is observed in the overdoped region.

In order to understand whether phonons can be responsible for peculiar shape of the ARPES in the undoped cuprates, the LF of an interacting with phonons hole in Mott insulator was studied by DMC-SO [49]. The case of the LF of a single hole corresponds to the ARPES in an undoped compound. For a system with large Hubbard repulsion U , when U is much larger than the typical bandwidth W of noninteracting QP, the problem reduces to the t - J model [181, 182, 158, 11]

$$\hat{H}_{t-J} = -t \sum_{\langle ij \rangle s} c_{is}^\dagger c_{js} + J \sum_{\langle ij \rangle} (\mathbf{S}_i \mathbf{S}_j - n_i n_j / 4) . \quad (39)$$

Here $c_{j\sigma}$ is projected (to avoid double occupancy) fermion annihilation operator, n_i (< 2) is the occupation number, \mathbf{S}_i is spin 1/2 operator, J is an exchange integral, and $\langle ij \rangle$ denotes nearest-neighbor sites in two dimensional square lattice. Different theoretical approaches revealed [158, 183, 53] basic properties of the LF. The LF has a sharp peak in the low energy part of the spectrum which disperses with a bandwidth $W_{J/t} \sim 2J$ and, therefore, the large QP width in experiment can not be explained. More complicated $tt't''$ - J model takes into account hoppings to the second t' and third t'' nearest neighbors and, hence, dispersion of the hole changes [184, 185, 186, 178, 179, 32]. However, for parameters, which are necessary for description of dispersion in realistic high T_c superconductors [31, 178], peak in the low energy part remains sharp and well defined for all momenta [187].

After expressing spin operators in terms of Holstein-Primakoff spin wave operators and diagonalizing the spin part of Hamiltonian (39) by Fourier and Bogoliubov transformations [188, 10, 189, 190], $tt't''$ - J Hamiltonian is reduced to the boson-holon model, where hole (annihilation operator is $h_{\mathbf{k}}$) with dispersion $\varepsilon(\mathbf{k}) = 4t' \cos(k_x) \cos(k_y) + 2t'' [\cos(2k_x) + \cos(2k_y)]$ propagates in the magnon (annihilation operator is $\alpha_{\mathbf{k}}$) bath

$$\hat{H}_{t-J}^0 = \sum_{\mathbf{k}} \varepsilon(\mathbf{k}) h_{\mathbf{k}}^\dagger h_{\mathbf{k}} + \sum_{\mathbf{k}} \omega_{\mathbf{k}} \alpha_{\mathbf{k}}^\dagger \alpha_{\mathbf{k}} \quad (40)$$

with magnon dispersion $\omega_{\mathbf{k}} = 2J \sqrt{1 - \gamma_{\mathbf{k}}^2}$, where $\gamma_{\mathbf{k}} = (\cos k_x + \cos k_y)/2$. The hole is scattered by magnons as described by

$$\hat{H}_{t-J}^{\text{h-m}} = N^{-1/2} \sum_{\mathbf{k}, \mathbf{q}} M_{\mathbf{k}, \mathbf{q}} \left[h_{\mathbf{k}}^\dagger h_{\mathbf{k}-\mathbf{q}} \alpha_{\mathbf{k}} + h.c. \right] \quad (41)$$

with the scattering vertex $M_{\mathbf{k}, \mathbf{q}}$. Parameters t , t' and t'' are hopping amplitudes to the first, second and third near neighbors, respectively. If hopping integrals t' and t'' are set to zero and bare hole has no dispersion, the problem (40-41) corresponds to t - J model.

Short range interaction of a hole with dispersionless optical phonons $\hat{H}^{\text{e-ph}} = \Omega_0 \sum_{\mathbf{k}} b_{\mathbf{k}}^\dagger b_{\mathbf{k}}$ of the frequency Ω_0 is introduced by Holstein Hamiltonian

$$\hat{H}^{\text{e-ph}} = N^{-1/2} \sum_{\mathbf{k}, \mathbf{q}} \frac{\sigma}{\sqrt{2M\Omega_0}} \left[h_{\mathbf{k}}^\dagger h_{\mathbf{k}-\mathbf{q}} b_{\mathbf{q}} + h.c. \right] , \quad (42)$$

where σ is the momentum and isotope independent coupling constant, M is the mass of the vibrating lattice ions, and Ω_0 is the frequency of dispersionless phonon. The coefficient in front of square brackets is the standard Holstein interaction constant $\gamma = \sigma / \sqrt{2M\Omega_0}$. In the following we characterize strength of EPI in terms of dimensionless coupling constant $\lambda = \gamma^2 / 4t\Omega_0$. Note, if interaction with magnetic subsystem (41) is neglected and hole dispersion $\varepsilon(\mathbf{k})$

is chosen in the form $\varepsilon(\mathbf{k}) = 2t[\cos(k_x) + \cos(k_y)]$, the problem (40), (42) corresponds to standard Holstein model where hole with near neighbor hopping amplitude t interacts with dispersionless phonons.

We consider the evolution of ARPES of a single hole in t - J -Holstein model (40)-(42) from the weak to the strong coupling regime and dispersion of the LF in the strong coupling regime in Sect. 6.1. It occurs that properties of the LF in the strong coupling regime of the EPI explain the puzzle of broad lineshape in ARPES in underdoped high T_c superconductors. Therefore, in order to suggest a crucial test for the mechanism of phonon-induced broadening, we present calculations of the effect of the isotope substitution on the ARPES in Sect. 6.2.

6.1 Spectral Function of a Hole Interacting with Phonons in the t - J Model: Self-Trapping and Momentum Dependence

Previously, the LF of t - J -Holstein model was studied by exact diagonalization method on small clusters [191] and in the non-crossing approximation (NCA)⁶ for both phonons and magnons [192, 193]. However, the small system size in exact diagonalization method implies a discrete spectrum and, therefore, the problem of lineshape could not be addressed. The latter method omits the FDs with mutual crossing of phonon propagators and, hence, is an invalid approximation for phonons in strong and intermediate couplings of EPI. This statement was demonstrated by DMC, which can sum all FDs for Holstein model both exactly and in the NCA [49]. Exact results and those of NCA are in good agreement for small values $\lambda \leq 0.4$ and drastically different for $\lambda > 1$. For example, for $\Omega_0/t = 0.1$ exact result shows a sharp crossover to strong coupling regime for $\lambda > \lambda_H^c \approx 1.2$ whereas NCA result does not undergo such crossover even at $\lambda = 100$. On the other hand, NCA is valid for interaction of a hole with magnons since spin $S=1/2$ can not flip more than once and number of magnons in the polaronic cloud can not be large. Note that the t - J -Holstein model is reduced to problem of polaron which interacts with several bosonic fields (3)-(4).

DMC expansion in [49] takes into account mutual crossing of phonon propagators and, in the framework of partial NCA, neglects mutual crossing of magnon propagators, to avoid sign problem. NCA for magnons is justified for $J/t \leq 0.4$ by good agreement of results of NCA and exact diagonalization on small clusters [188, 10, 194, 195, 190]. Recently results of exact diagonalization were compared in the limit of small EPI for t - J -Holstein model, boson-holon model (40-42) without NCA, and boson-holon model with NCA [196]. Although agreement is not so good as for pure t - J model, it was concluded that NCA for magnons is still good enough to suggest that one can use NCA for a qualitative description of the t - J -Holstein model.

⁶ NCA is equivalent to self-consistent Born approximation (SCBA)

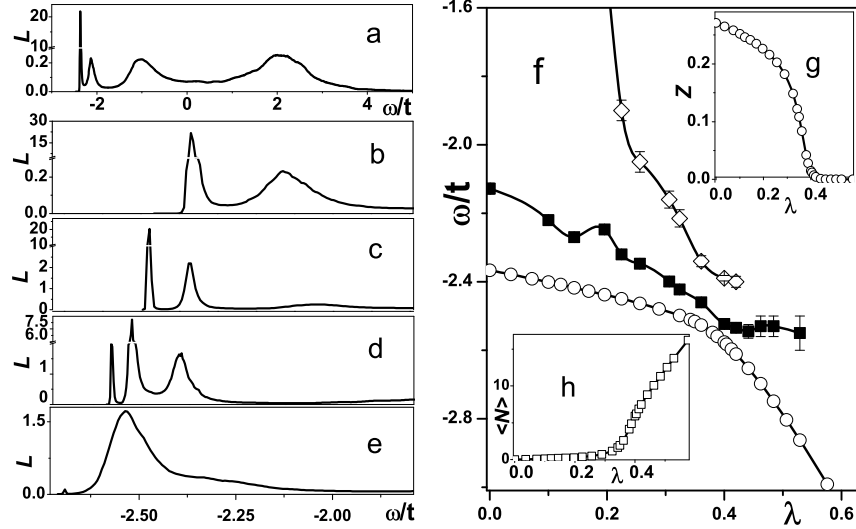


Fig. 10. (a) The LF of a hole in the ground state $\mathbf{k} = (\pi/2, \pi/2)$ at $J/t = 0.3$ and $\lambda = 0$. Low energy part of the LF of a hole in the ground state $\mathbf{k} = (\pi/2, \pi/2)$ at $J/t = 0.3$: (b) $\lambda = 0$; (c) $\lambda = 0.3$; (d) $\lambda = 0.4$; (e) $\lambda = 0.46$. Dependence on coupling strength λ at $J/t = 0.3$: (f) energies of lowest LF resonances; (g) Z -factor of lowest peak; (h) average number of phonons $\langle N \rangle$.

Figures 10a-e show low energy part of LF in the ground state at $\mathbf{k} = (\pi/2, \pi/2)$ in the weak, intermediate, and strong coupling regimes of interaction with phonons. Dependence on the coupling constant of energies of resonances (Fig. 10f), $Z^{\mathbf{k}=(\pi/2, \pi/2)}$ -factor of lowest peak (Fig. 10g), and average number of phonons in the polaronic cloud $\langle N \rangle$ (Fig. 10h) demonstrates a picture which is typical for ST (see [80, 54] and Sect. 4). Two states cross and hybridize in the vicinity of critical coupling constant $\lambda_{t-J}^c \approx 0.38$, $Z^{\mathbf{k}=(\pi/2, \pi/2)}$ -factor of lowest resonance sharply drops and average number of phonons in polaronic cloud quickly rises. According to the general understanding of the ST phenomenon, above the critical couplings $\lambda > \lambda_{t-J}^c$ one expects that the lowest state is dispersionless while the upper one has small effective mass. This assumption is supported by the momentum dependence of the LF in the strong coupling regime (Fig. 11a-e). Dispersion of upper broad shake-off Franck-Condon peak nearly perfectly obeys relation

$$\varepsilon_{\mathbf{k}} = \varepsilon_{min} + W_{J/t}/5 \{ [\cos k_x + \cos k_y]^2 + [\cos(k_x + k_y) + \cos(k_x - k_y)]^2 / 4 \}, \quad (43)$$

which describes dispersion of the pure t - J model in the broad range of exchange constant $0.1 < J/t < 0.9$ [194] (Fig. 11f). Note that this property of the shake-off peak is general for the whole strong coupling regime (Fig. 11f).

Momentum dependence of the shake-off peak, reproducing that of the free particle, is the direct consequence of the adiabatic regime. Actually, phonon frequency Ω_0 is much smaller than the coherent bandwidth $2J$ of the t - J

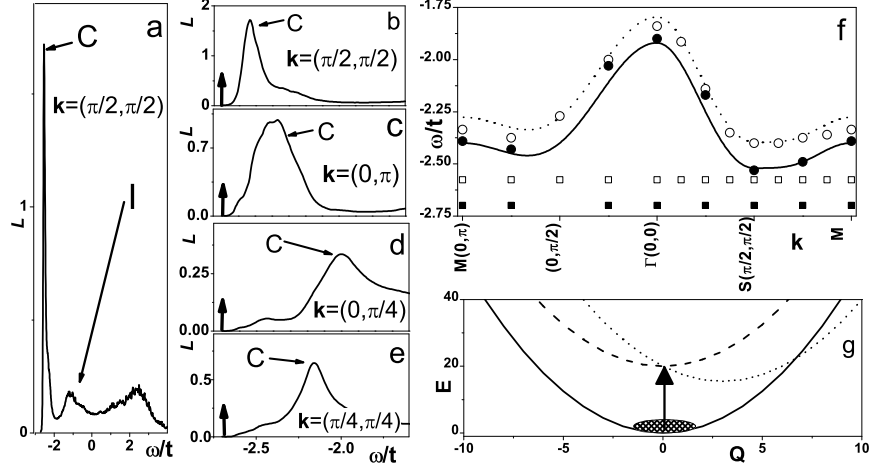


Fig. 11. The LF of a hole at $J/t = 0.3$ and $\lambda = 0.46$: (a) full energy range for $\mathbf{k} = (\pi/2, \pi/2)$; (b–e) low energy part for different momenta. Slanted arrows show broad peaks which can be interpreted in ARPES spectra as coherent (C) and incoherent (I) part. Vertical arrows in panels (b)–(e) indicate position of “invisible” lowest resonance. (f) Dispersion of resonances energies at $J/t = 0.3$: broad resonance (filled circles) and lowest polaron pole (filled squares) at $\lambda = 0.46$; broad resonance (open circles) and lowest polaron pole (open squares) at $\lambda = 0.4$. The solid curves are dispersions (43) of a hole in pure t - J model at $J/t = 0.3$ ($W_{J/t=0.3} = 0.6$): $\varepsilon_{min} = -2.396$ ($\varepsilon_{min} = -2.52$) for dotted (solid) line. Panel (g) shows ground state potential $Q^2/2$ (solid line), excited state potential without relaxation $D + Q^2/2$ (dashed line), and relaxed excited state potential $D + (Q - \lambda)^2/2 - \lambda^2/2$ (dotted line).

model, giving the adiabatic ratio $\Omega/2J = 1/6 \ll 1$. Besides, as experience with the OC of the Fröhlich polaron (Sect. 3.2) shows, there is one more important parameter in the strong coupling limit. Namely, the ratio between measurement process time $\tau_{mp} = \hbar/\Delta E$ where ΔE is the energy separation of shake-off hump from the ground state pole, and that of characteristic lattice time $\tau \approx 1/\Omega_0$ is much less than unity. Hence, fast photoemission probe sees the ions frozen in one of possible configurations [197]. The LF in the FC limit is a sum of transitions between a lower $E_{low}(Q)$ and an upper $E_{up}(Q)$ sheets of adiabatic potential, weighted by the adiabatic wave function of the lower sheet $|\psi_{low}(Q)|^2$ [198]. If EPI is absent both in initial $E_{low}(Q) = Q^2/2$ and final $E_{up}(Q) = D + Q^2/2$ states, the LF is peaked at the energy D . Then, if there is EPI $\Delta E_{up}(Q) = -\lambda Q$ only in the final state, i.e. when hole is removed from the Mott insulator, the upper sheet of adiabatic potential $E_{up}(Q) = D - \lambda^2/2 + (Q - \lambda)^2/2$ has the same energy D at $Q = 0$. Since the probability function $|\psi_{low}(Q)|^2$ has maximum at $Q = 0$, the peak of the LF broadens but its energy does not shift [198] (Fig. 11g).

Behavior of the LF is the same as observed in the ARPES of undoped cuprates. The LF consists of a broad peak and a high energy incoherent continuum (see Fig. 11a). Besides, dispersion of the broad peak “c” in Figs. 11 reproduces that of sharp peak in pure t - J model (Fig. 11b-f). The lowest dispersionless peak, corresponding to small radius polaron, has very small weight and, hence, can not be seen in experiment. On the other hand, according to experiment, momentum dependence of spectral weight $Z^{(\mathbf{k})}$ of broad resonance exactly reproduces dispersion of $Z^{(\mathbf{k})}$ -factor of pure t - J model. The reason for such perfect mapping is that in adiabatic case $\Omega_0/2J \ll 1$ all weight of the sharp resonance in t - J model without EPI is transformed at strong EPI into the broad peak. This picture implies that the chemical potential in the heavily underdoped cuprates is not connected with the broad resonance but pinned to the real quasiparticle pole with small Z -factor. This conclusion was recently confirmed experimentally [177].

Comparing the critical EPI for a hole in the t - J -Holstein model (40-42) $\lambda_{t-J}^c \approx 0.38$ and that for Holstein model $\lambda_H^c \approx 1.2$ with the same value of hopping t , we conclude that *spin-hole interaction accelerates transition into the strong coupling regime*. The reason for enhancement of the role of EPI is found in [196]. Comparison of the EPI driven renormalization of the effective mass in t - J -Holstein and Holstein model shows that large effective mass in the t - J model is responsible for this effect. The enhancement of the role of EPI by EEI takes place at least for a single hole at the bottom of the t - J band. Had the comparison been made with half-filled model, the result would have been smaller enhancement or no enhancement at all [199]. On the other hand, coupling constant of half-breathing phonon is increased by correlations [200]. Finally, we conclude that effect of enhancement of the effective EPI by EEI is not unambiguous and depends on details of interaction and filling. However, this effect is present for small filling in the t - J -Holstein model.

6.2 Isotope Effect on ARPES in Underdoped High-Temperature Superconductors

The magnetic resonance mode and the phonon modes are the two major candidates to explain the “kink” structure of the electron energy dispersion around 40-70 meV below the Fermi energy, and the isotope effect (IE) on ARPES should be the smoking-gun experiment to distinguish between these two. Gweon et al. [201] performed the ARPES experiment on O¹⁸-replaced Bi2212 at optimal doping and found an appreciable IE, which however can not be explained within the conventional weak-coupling Migdal-Eliashberg theory. Namely the change of the spectral function due to O¹⁸-replacement has been observed at higher energy region beyond the phonon energy (~ 60 meV). This is in sharp contrast to the weak coupling theory prediction, i.e., the IE should occur only near the phonon energy. Hence the IE in optimal Bi2212 remains still a puzzle. On the other hand, the ARPES in undoped materials, as described in Sect. 6.1, has recently been understood in terms of

the small polaron formation [49, 202, 198]. Therefore, it is essential to compare experiment in undoped systems with presented in this Sect. DMC-SO data, where theory can offer quantitative results.

In addition to high- T_c problem, strong EPI mechanism of ARPES spectra broadening was considered as one of alternative scenarios for diatomic molecules [203], colossal magnetoresistive manganites [34], quasi-one-dimensional Peierls conductors [37, 38], and Verwey magnetites [39]. Therefore, exact analysis of the IE on ARPES at strong EPI is of general interest for conclusive experiments in a broad variety of compound classes.

Dimensionless coupling constant $\lambda = \gamma^2/4t\Omega$ in (42) is an invariant quantity for the simplest case of IE. Indeed, assuming natural relation $\Omega \sim 1/\sqrt{M}$ between phonon frequency and mass, we find that λ does not depend on the isotope factor $\kappa_{\text{iso}} = \Omega/\Omega_0 = \sqrt{M_0/M}$, which is defined as the ratio of phonon frequency in isotope substituted (Ω) and normal (Ω_0) systems. We chose adopted parameters of the $tt't''$ - J model which reproduce the experimental dispersion of ARPES [178]: $J/t = 0.4$, $t'/t = -0.34$, and $t''/t = 0.23$. The frequency of the relevant phonon [32] is set to $\Omega_0/t = 0.2$ and the isotope factor $\kappa_{\text{iso}} = \sqrt{16/18}$ corresponds to substitution of O^{18} isotope for O^{16} .

To sweep aside any doubts of possible instabilities of analytic continuation, we calculate the LF for normal compound ($\kappa_{\text{nor}} = 1$), isotope substituted ($\kappa_{\text{iso}} = \sqrt{16/18}$) and “anti-isotope” substituted ($\kappa_{\text{ant}} = \sqrt{18/16}$) compounds. Monotonic dependence of LF on κ ensures stability of analytic continuation and gives possibility to evaluate the error-bars of a quantity \mathcal{A} using quantities $\mathcal{A}_{\text{iso}} - \mathcal{A}_{\text{nor}}$, $\mathcal{A}_{\text{nor}} - \mathcal{A}_{\text{ant}}$, and $(\mathcal{A}_{\text{iso}} - \mathcal{A}_{\text{ant}})/2$.

Since LF is sensitive to strengths of EPI only for low frequencies [55], we concentrate on the low energy part of the spectrum. Figure 12 shows IE on the hole LF for different couplings in nodal and antinodal points, respectively. The general trend is a shift of all spectral features to larger energies with increase of the isotope mass ($\kappa < 1$). One can also note that the shift of broad FCP is much larger than that of narrow real-QP peak. Moreover, for large couplings λ the shift of QP energy approaches zero and only decrease of QP spectral weight Z is observed for larger isotope mass. On the other hand, the shift of FCP is not suppressed for larger couplings. Except for the LF in nodal point at $\lambda = 0.62$ (Fig. 12a, b), where LF still has significant weight of QP δ -functional peak, there is one more notable feature of the IE. With increase of the isotope mass the height of FCP increases. Taking into account the conservation law for LF $\int_{-\infty}^{+\infty} L_{\mathbf{k}}(\omega) = 1$ and insensitivity of high energy part of LF to EPI strength [55], the narrowing of the FCP for larger isotope mass can be concluded. To understand the trends of the IE in the strong coupling regime we analyze the exactly solvable independent oscillators model (IOM) [60]. The LF in IOM is the Poisson distribution

$$L(\omega) = \exp[-\xi_0/\kappa] \sum_{l=0}^{\infty} \frac{[\xi_0/\kappa]^l}{l!} \mathcal{G}_{\kappa,l}(\omega), \quad (44)$$

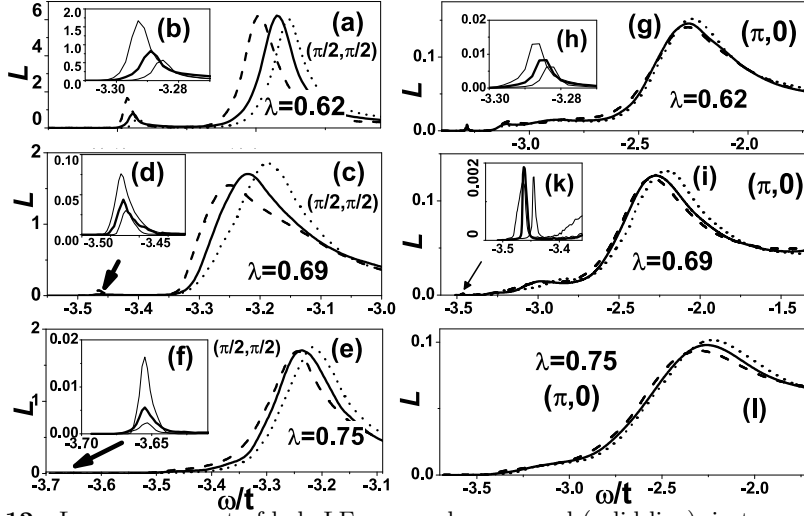


Fig. 12. Low energy part of hole LFs: normal compound (solid line), isotope substituted compound (dotted line) and “antiisotope” substituted compound (dashed line). LFs at different couplings in the nodal (a, c, e) and antinodal (g, i, l) points. Insets (b, d, f, h, k) show low energy peak of real QP.

where $\xi_0 = \gamma_0^2/\Omega_0^2 = 4t\lambda/\Omega_0$ is dimensionless coupling constant for normal system and $\mathcal{G}_{\kappa,l}(\omega) = \delta[\omega + 4t\lambda - \Omega_0\kappa l]$ is the δ -function. The properties of the Poisson distribution quantitatively explain many features of the IE on LF⁷.

The energy $\omega_{\text{QP}} = -4t\lambda$ of the zero-phonon line $l = 0$ in (44) depends only on isotope independent quantities which explains very weak isotope dependence of QP peak energy in insets of Fig. 12. Besides, change of the zero-phonon line weight $Z^{(0)}$ obeys relation $Z_{\text{iso}}^{(0)}/Z_{\text{nor}}^{(0)} = \exp[-\xi_0(1 - \kappa)/\kappa]$ in IOM. These IOM estimates agree with DMC data within 15% in the nodal point and within 25% in the antinodal one. IE on FCP in the strong coupling regime follows from the properties of zero $M_0 = \int_{-\infty}^{+\infty} L(\omega)d\omega = 1$, first $M_1 = \int_{-\infty}^{+\infty} \omega L(\omega)d\omega = 0$, and second $M_2 = \int_{-\infty}^{+\infty} \omega^2 L(\omega)d\omega = \kappa\xi_0\Omega_0^2$ moments of shifted Poisson distribution (44). Moments M_0 and M_2 establish relation $\mathcal{D} = h_{\text{iso}}^{\text{FCP}}/h_{\text{nor}}^{\text{FCP}} = 1/\sqrt{\kappa} \approx 1.03$ between heights of FCP in normal and substituted compounds. DMC data in the antinodal point perfectly agree with the above estimate for all couplings. This is consistent with the idea that the anti-nodal region remains in the strong coupling regime even though the nodal region is in the crossover region. In the nodal point DMC data well agree with IOM estimate for $\lambda = 0.75$ ($\mathcal{D} \approx 1.025$) whereas at $\lambda = 0.69$ and

⁷ Cautions should be made about approximate form of EPI (42). Strictly speaking, actual momentum dependence of the interaction constant σ [204, 205] can slightly change the obtained differences between nodal and antinodal points though the general trends have to be left intact because ST is caused solely by the short range part of EPI [80].

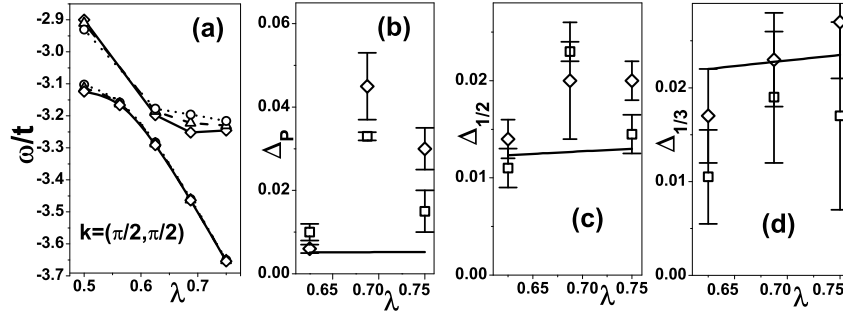


Fig. 13. (a) Energies of ground state and broad peaks for normal (triangles), isotope substituted (circles) and “antiisotope” substituted (diamonds) compounds. Comparison of IOM estimates (lines) with DMC data in the nodal (squares) and antinodal (diamonds) points: (b) shift of the FCP top, (c) FCP leading edge at 1/2 of height, and (d) FCP leading edge at 1/3 of height.

$\lambda = 0.62$ influence of the ST point leads to anomalous values of \mathcal{D} : $\mathcal{D} \approx 1.07$ and $\mathcal{D} \approx 0.98$, respectively. Shift of the low energy edge at half maximum $\Delta_{1/2}$ must be proportional to change of the root square of second moment $\Delta_{\sqrt{M_2}} = \sqrt{\xi_0} \Omega_0 [1 - \sqrt{\kappa}]$. As we found in numeric simulations of (44) with Gaussian functions⁸ $\mathcal{G}_{\kappa,l}(\omega)$, relation $\Delta_{1/2} \approx \Delta_{\sqrt{M_2}}/2$ is accurate to 10% for $0.62 < \lambda < 0.75$. Also, simulations show that the shift of the edge at one third of maximum $\Delta_{1/3}$ obeys relation $\Delta_{1/3} \approx \Delta_{\sqrt{M_2}}$. DMC data with IOM estimates are in good agreement for strong EPI $\lambda = 0.75$ (Fig. 13). However, shift of the FCP top Δ_p and $\Delta_{1/2}$ are considerably enhanced in the self-trapping (ST) transition region. The physical reason for enhancement of IE in this region is a general property regardless of the QP dispersion, range of EPI, etc. The influence of nonadiabatic matrix element, mixing excited and ground states, on the energies of resonances essentially depends on the phonon frequency. While in the adiabatic approximation ST transition is sudden and nonanalytic in λ [80], nonadiabatic matrix elements turn it to smooth crossover [144]. Thus, as illustrated in Fig. 13a, the smaller the frequency the sharper the kink in the dependence of excited state energy on the interaction constant

In the undoped case the present results can be directly compared with the experiments. It is found that the IE on the ARPES lineshape of a single hole is anomalously enhanced in the intermediate coupling regime while can be described by the simple independent oscillators model in the strong coupling regime. The shift of FCP top and change of the FCP height are relevant quantities to pursue experimentally in the intermediate coupling regime since IE on these characteristics is enhanced near the self trapping point. In

⁸ Results are almost independent on the parameter η of the Gaussian distribution $\mathcal{G}_{\kappa,l}(\omega) = 1/(\eta\sqrt{2\pi}) \exp(-[\omega + 4t\lambda - \Omega_0\kappa l]/(2\eta^2))$ in the range [0.12, 0.2].

contrast, shift of the leading edge of the broad peak is the relevant quantity in the strong coupling regime since this value increases with coupling as $\sqrt{\lambda}$. These conclusions, depending on the fact whether self trapping phenomenon is encountered in specific case, can be applied fully or partially to another compounds with strong EPI [34, 37, 38, 39].

6.3 Conclusions and Perspectives

In this article, we have focused mainly on the polaron problem in strongly correlated systems. This offers an approach from the limit of low carrier concentration doped into the (Mott) insulator, which is complementary to the conventional Eliashberg-Migdal approach for the EPI in metals. In the latter case, we have the Fermi energy ε_F as a relevant energy scale, which is usually much larger than the phonon frequency Ω_0 . In this case, the adiabatic Migdal approximation is valid and the vertex corrections, which correspond to the multi-phonon cloud and are essential to the self-trapping phenomenon, are suppressed by the ratio Ω_0/ε_F . Therefore an important issue is the crossover from the strong coupling polaronic picture to the weak coupling Eliashberg-Migdal picture. This occurs as one increases the carrier doping into the insulator. As is observed by ARPES experiments in high temperature superconductors, the polaronic states continue to survive even at finite doping [177]. This suggests a novel polaronic metallic state in underdoped cuprates, which is common also in CMR manganites [36] and is most probably universal in transition metal oxides. In the optimal and overdoped region, the Eliashberg-Migdal picture becomes appropriate [170, 171], but still a nontrivial feature of the EPI is its strong momentum dependence leading to the dichotomy between the nodal and anti-nodal regions. It is an interesting observation that the highest superconducting transition temperature is attained at the crossover region between the two pictures above, which suggests that both the itinerancy and strong coupling to the phonons are essential to the quantum coherence. It should be noted that this crossover occurs in a nontrivial way also in the momentum space, i.e., the nodal and anti-nodal regions behave quite differently as discussed in Sect. 6.2. However, the relevance of the EPI to the high T_c superconductivity is still left for future investigations.

We hope that this article convinces the readers the vital role of ARPES experiments and numerically exact solutions to the EPI problem, the combination of them offers a powerful tool for the momentum-energy resolved analysis of these rather complicated strongly correlated electronic systems. This will pave a new path to the deeper understanding of the many-body electronic systems.

We thank Y. Toyozawa, Z. X. Shen, T. Cuk, T. Devereaux, J. Zaanen, S. Ishihara, A. Sakamoto, N. V. Prokofev, B. V. Svistunov, E. A. Burovski, J. T. Devreese, G. de Filippis, V. Cataudella, P. E. Kornilovitch, O. Gunnarsson, N. M. Plakida, and K. A. Kikoin, for collaborations and discussions.

References

1. J. Appel: *Solid State Physics*, Vol. 21, ed by H. Ehrenreich, F. Seitz and D. Turnbull (Academic, New York 1968).
2. S. I. Pekar: *Untersuchungen über die Elektronentheorie der Kristalle*, (Akademie Verlag, Berlin 1954)
3. L. D. Landau: *Sov. Phys.* **3**, 664 (1933).
4. H. Fröhlich, H. Pelzer, S. Zienau: *Philos. Mag.* **41**, 221 (1950)
5. J. T. Devreese: *Encyclopedia of Applied Physics* Vol. 14, ed by G. L. Trigg (VCH, New York 1996), p. 383
6. A. I. Anselm, Yu. A. Firsov: *J. Exp. Theor. Phys.* **28**, 151 (1955); *ibid.* **30**, 719 (1956)
7. M. Ueta, H. Kanzaki, K. Kobayashi, Y. Toyozawa, E. Hanamura: *Excitonic Processes in Solids*, (Springer-Verlag, Berlin 1986)
8. Y. Toyozawa: *Progr. Theor. Phys.* **20** 53 (1958).
9. Y. Toyozawa: *Optical Processes in Solids*, (University Press, Cambridge 2003)
10. C. L. Kane, P. A. Lee, N. Read: *Phys. Rev. B* **39**, 6880 (1989)
11. Yu. A. Izyumov: *Usp. Fiz. Nauk* **167**, 465 (1997) [*Physics-Uspekhi* **40**, 445 (1997)]
12. J. Kanamori: *Appl. Phys.* **31**, S14 (1960).
13. A. Abragam, B. Bleaney: *Electron Paramagnetic Resonance of Transition Ions*, (Clarendon Press, Oxford 1970)
14. K. I. Kugel, D. I. Khomskii: *Sov. Phys. Usp.* **25**, 231 (1982)
15. A. J. Millis, P. B. Littlewood, B. I. Shraiman: *Phys. Rev. Lett.* **74**, 5144 (1995)
16. A. S. Alexandrov, A. M. Bratkovsky: *Phys. Rev. Lett.* **82**, 141 (1999)
17. E. I. Rashba: *Sov. Phys. JETP* **23**, 708 (1966)
18. Y. Toyozawa, J. Hermanson: *Phys. Rev. Lett.* **21**, 1637 (1968)
19. I. B. Bersuker: *The Jahn-Teller Effect*, (IFI/Plenum, New York 1983)
20. V. L. Vinetskii: *Zh. Exp. Teor. Fiz* **40**, 1459 (1961) [*Sov. Phys. - JETP* **13**, 1023 (1961)]
21. P. W. Anderson: *Phys. Rev. Lett.* **34** 953 (1975)
22. H. Hiramoto, Y. Toyozawa: *J. Phys. Soc. Jpn.* **54**, 245 (1985)
23. A. Alexandrov, and J. Ranninger: *Phys. Rev. B* **23** 1796 (1981)
24. A. Alexandrov, and J. Ranninger: *Phys. Rev. B* **24** 1164 (1981)
25. H. Haken: *Il Nuovo Cimento* **3**, 1230 (1956)
26. F. Bassani, G. Pastori Parravicini: *Electronic States and Optical Transitions in Solids*, (Pergamon, Oxford 1975)
27. J. Pollman, H. Büttner: *Phys. Rev. B* **16**, 4480 (1977)
28. A. Sumi: *J. Phys. Soc. Jpn.* **43**, 1286 (1977)
29. Y. Shinozuka, Y. Toyozawa: *J. Phys. Soc. Jpn.* **46**, 505 (1979)
30. Y. Toyozawa: *Physica* **116B**, 7 (1983)
31. B. O. Wells, Z.-X. Shen, A. Matsuura et al: *Phys. Rev. Lett.* **74**, 964 (1995)
32. A. Danmascelli, Z.-X. Shen, and Z. Hussain: *Rev. Mod. Phys.* **75**, 473 (2003)
33. X. J. Zhou, T. Yoshida, D.-H. Lee et al: *Phys. Rev. Lett.* **92**, 187001 (2004)
34. D. S. Dessau, T. Saitoh, C.-H. Park et al: *Phys. Rev. Lett.* **81**, 192 (1998);
35. N. Mannella, A. Rosenhahn, C. H. Booth et al: *Phys. Rev. Lett.* **92**, 166401 (2004)
36. N. Mannella, W. L. Yang, X. J. Zhou et al: *Nature* **438**, 474 (2005)
37. L. Perfetti, H. Berger, A. Reggiani et al: *Phys. Rev. Lett.* **87**, 216404 (2001)

38. L. Perfetti, S. Mitrovic, G. Margaritondo et al: Phys. Rev. B **66**, 075107 (2002)
39. D. Schrupp, M. Sing, M. Tsunekawa et al: Eur. Phys. Lett. **70**, 789 (2005)
40. R. J. McQueeney, T. Egami, G. Shirane and Y. Endoh: Phys. Rev. B **54** R9689 (1996)
41. H. A. Mook, R. M. Nicklow: Phys. Rev. B **20** 1656 (1979)
42. H. A. Mook, D. B. McWhan, F. Holtzberg: Phys. Rev. B **25** 4321 (1982)
43. N. V. Prokof'ev, B. V. Svistunov, I. S. Tupitsyn: J. Exp. Theor. Phys. **114**, 570 (1998) [Sov. Phys. - JETP **87**, 310 (1998)]
44. N. V. Prokof'ev, B. V. Svistunov: Phys. Rev. Lett. **81**, 2514 (1998)
45. A. S. Mishchenko, N. V. Prokof'ev, A. Sakamoto, B. V. Svistunov: Phys. Rev. B **62**, 6317 (2000)
46. E. A. Burovski, A. S. Mishchenko, N. V. Prokof'ev, B. V. Svistunov: Phys. Rev. Lett. **87**, 186402 (2001)
47. A. S. Mishchenko, N. Nagaosa, N. V. Prokof'ev, B. V. Svistunov, E. A. Burovski: Nonlinear Optics **29**, 257 (2002)
48. A. S. Mishchenko, N. Nagaosa, N. V. Prokof'ev, A. Sakamoto, B. V. Svistunov: Phys. Rev. Lett. **91**, 236401 (2003)
49. A. S. Mishchenko, N. Nagaosa: Phys. Rev. Lett. **93**, 036402 (2004)
50. A. S. Mishchenko: Usp. Phys. Nauk **175**, 925 (2005) [Physics-Uspeski **48**, 887 (2005)]
51. A. S. Mishchenko, N. Nagaosa: J. Phys. Soc. J. **75**, 011003 (2006)
52. A. S. Mishchenko, N. Nagaosa: Phys. Rev. Lett. **86**, 4624 (2001)
53. A. S. Mishchenko, N. V. Prokof'ev, B. V. Svistunov: Phys. Rev. B **64**, 033101 (2001)
54. A. S. Mishchenko, N. Nagaosa, N. V. Prokof'ev, A. Sakamoto, B. V. Svistunov: Phys. Rev. B **66** 020301 (2002)
55. A. S. Mishchenko, N. Nagaosa: Phys. Rev. B **73**, 092502 (2006)
56. A. S. Mishchenko, N. Nagaosa: J. Phys. Chem. Solids **67**, 259 (2006)
57. G. De Filippis, V. Cataudella, A. S. Mishchenko, J. T. Devreese, C. A. Perroni: Phys. Rev. Lett. **96**, 136405 (2006)
58. J. T. Devreese: Optical Properties of Few and Many Fröhlich Polarons from 3D to 0D, contribution to the present book.
59. A. A. Abrikosov, L. P. Gor'kov, I. E. Dzyaloshinskii: *Quantum field theoretical method in statistical physics* (Pergamon Press, Oxford 1965)
60. G. D. Mahan: *Many particle physics* (Plenum Press, Plenum Press 2000)
61. M. Jarrell, J. Gubernatis: Phys. Rep. **269**, 133 (1996)
62. R. Knox: *Theory of Excitons*, (Academic Press, New York 1963)
63. I. Egri: Phys. Rep **119**, 364 (1985)
64. D. Haarer: Chem. Phys. Lett **31**, 192 (1975)
65. D. Haarer, M. R. Philpot, H. Morawitz: J. Chem. Phys **63**, 5238 (1975)
66. A. Elscner, G. Weiser: Chem. Phys **98** 465 (1985)
67. J. I. Frenkel: Phys. Rev. **17**, 17 (1931)
68. J. H. Wannier: Phys. Rev. **52**, 191 (1937)
69. G. De Filippis, V. Cataudella, V. Marigliano Ramaglia, C. A. Perroni: Phys. Rev. B **72**, 014307 (2005)
70. M. Berciu: cond-mat/0602195
71. J. T. Devreese, L. F. Lemmens, J. Van Royen: Phys. Rev. B **15**, 1212 (1977)
72. P. E. Kornilovitch: Europhys. Lett. **59**, 735 (2002)
73. J. Devreese, R. Evrard: Phys. Lett. **11**, 278 (1966)

74. E. Kartheuzer, R. Evrard, J. Devreese: Phys. Rev. Lett. **22**, 94 (1969)
75. J. Devreese, J. De Sitter, M. Goovaerts: Phys. Rev. B **5**, 2367 (1972)
76. J. T. Devreese: Internal structure of free Fröhlich polarons, optical absorption and cyclotron resonance. In *Polarons in Ionic crystals and Polar Semiconductors* (North Holland, Amsterdam 1972) pp 83–159
77. M. J. Goovaerts, J. M. De Sitter, J. T. Devreese: Phys. Rev. B **7**, 2639 (1973)
78. R. Feynman, R. Hellwarth, C. Iddings, and P. Platzman: Phys. Rev. **127**, 1004 (1962)
79. T. D. Lee, F. E. Low, D. Pines: Phys. Rev. **90**, 297 (1953)
80. E. I. Rashba: Self-trapping of excitons. In *Modern Problems in Condensed Matter Sciences*, vol. 2, ed by V. M. Agranovich and A. A. Maradudin (North Holland, Amsterdam 1982) pp 543–602
81. N. Metropolis, A. W. Rosenbluth, M. N. Rosenbluth, A. M. Teller and E. Teller: J. Chem. Phys. **21**, 1087 (1953)
82. D. P. Landau, K. Binder: *A Guide to Monte Carlo Simulations in Statistical Physics*, (University Press, Cambridge 2000)
83. A. W. Sandvik, J. Kurkijärvi: Phys. Rev. B **43**, 5950 (1991)
84. A. N. Tikhonov, V. Y. Arsenin: *Solutions of Ill-Posed Problems*, (Winston, Washington 1977)
85. E. Perchik: math-ph/0302045
86. D. L. Phillips: J. Assoc. Comput. Mach. **9** 84 (1962)
87. A. N. Tikhonov: DAN USSR **151** 501 (1963)
88. S. S. Aplesnin: J. Exp. Theor. Phys **97** 969 (2003)
89. G. Onida, L. Reining, A. Rubio: Rev. Mod. Phys. **74**, 601 (2002)
90. L. J. Sham, T. M. Rice: Phys. Rev. **144**, 708 (1965).
91. L. X. Benedict, E. L. Shirley, R. B. Bohn: Phys. Rev. Lett. **80**, 4514 (1998)
92. S. Albrecht, L. Reining, R. Del Sole, G. Onida: Phys. Rev. Lett. **80**, 4510 (1998)
93. M. Rohlfing, S. G. Louie: Phys. Rev. Lett. **81**, 2312 (1998)
94. A. Marini, R. Del Sole: Phys. Rev. Lett. **91**, 176402 (2003)
95. W. Stephan: Phys. Rev. B **54**, 8981 (1996)
96. G. Wellein, H. Fehske: Phys. Rev. B **56**, 4513 (1997)
97. H. Fehske, J. Loos, G. Wellein: Z. Phys. B **104**, 619 (1997)
98. H. Fehske, J. Loos, G. Wellein: Phys. Rev. B **61**, 8016 (2000)
99. J. Bonča, S. A. Trugman, I. Batistić: Phys. Rev. B **60**, 1633 (1999)
100. L.-C. Ku, S. A. Trugman, J. Bonča: Phys. Rev. B **65**, 174306 (2002)
101. S. E. Shawish, J. Bonča, L.-C. Ku, S. A. Trugman: Phys. Rev. B **67**, 014301 (2003)
102. O. S. Barisic: Phys. Rev. B **65**, 144301 (2002)
103. O. S. Barisic: Phys. Rev. B **69**, 064302 (2004)
104. A. Georges, G. Kotliar: Phys. Rev. B **45**, 647 (1992)
105. M. Jarrel: Phys. Rev. Lett. **69**, 168 (1992)
106. P. G. J. van Dongen, D. Vollhardt: Phys. Rev. Lett. **65**, 1663 (1990)
107. A. Georges, G. Kotliar, W. Krauth, M. J. Rozenberg: Rev. Mod. Phys. **68**, 13 (1996)
108. S. Ciuchi, F. de Pasquale, S. Fratini, D. Feinberg: Phys. Rev. B **56** 4494 (1997)
109. D. Sénéchal, D. Perez, M. Pioro-Landrière: Phys. Rev. Lett. **84**, 522 (2000)
110. D. Sénéchal, D. Perez, M. Plouffe: Phys. Rev. B **66**, 075129 (2002)
111. M. Hohenadler, M. Aichhorn, W. von der Linden: Phys. Rev. B **68**, 18430 (2003)

112. M. Hohenadler, M. Aichhorn, W. von der Linden: Phys. Rev. B **71**, 014302 (2005)
113. M. Hohenadler, D. Neuber, W. von der Linden, G. Wellein, J. Loos, H. Fehske: *ibid.* **71**, 245111 (2005)
114. S. R. White: Phys. Rev. Lett. **69**, 2863 (1992)
115. S. R. White: Phys. Rev. B **48**, 10345 (1993)
116. S. R. White: Phys. Rev. Lett. **77**, 363 (1996)
117. E. Jeckelmann, S. R. White: Phys. Rev. B **57**, 6376 (1998)
118. G. Hager, G. Wellein, E. Jeckelmann, H. Fehske: Phys. Rev. B **71**, 075108 (2005)
119. P. E. Kornilovitch: Phys. Rev. Lett. **81**, 5382 (1998)
120. P. E. Kornilovitch: Phys. Rev. B **60**, 3237 (1999)
121. P. E. Spenser, J. H. Samson, P. E. Kornilovitch, A. S. Alexandrov: Phys. Rev. B **71**, 184310 (2005)
122. J. P. Hague, P. E. Kornilovitch, A. S. Alexandrov, J. H. Samson: Phys. Rev. B **73**, 054303 (2006)
123. A. S. Alexandrov, P. E. Kornilovitch: Phys. Rev. Lett. **82**, 807 (1999)
124. A. S. Alexandrov, P. E. Kornilovitch: Phys. Rev. B **70**, 224511 (2004)
125. S. Ciuchi, F. de Pasquale, D. Feinberg: Europhys. Lett. **30**, 151 (1995)
126. A. S. Alexandrov, V. V. Labanov, D. K. Ray: Phys. Rev. B **49**, 9915 (1994)
127. A. S. Alexandrov, J. Ranninger: Phys. Rev. B **45**, 13109 (1992)
128. L. D. Landau, S. I. Pekar: Zh. Eksp. Teor. Fiz. **18**, 419 (1948) [Sov. Phys. JETP **18**, 341 (1948)]
129. V. L. Gurevich, I. G. Lang, Yu. A. Firsov: Fiz. Tverd. Tela (Leningrad) **4**, 1252 (1962) [Sov. Phys. Solid State **4**, 918 (1962)]
130. J. Franck, E. G. Dymond: Trans. Faraday Soc. **21**, 536 (1926)
131. E. U. Condon: Phys. Rev. **32**, 858 (1928)
132. D. N. Bertran, J. J. Hopfield: J. Chem. Phys. **81**, 5753 (1984)
133. X. Urbain, B. Fabre, E. M. Staiace-Casagrande et al: Phys. Rev. Lett. **92**, 163004 (2004)
134. M. Lax: J. Chem. Phys. **20**, 1752 (1952)
135. D. I. Khomskii: Usp. Fiz. Nauk **129**, 443 (1979) [Sov. Phys. Usp. **22**, 879 (1979)]
136. C. E. T. Goncalves da Silva, L. M. Falicov: Phys. Rev. B **13**, 3948 (1976).
137. P. A. Alekseev, J. M. Mignot, J. Rossat-Mignot: J. Phys.: Condens. Matter **7**, 289 (1995)
138. K. A. Kikoin, A. S. Mishchenko: J. Phys.: Condens. Matter **7**, 307 (1995)
139. R. Feynman: Phys. Rev. **97**, 660 (1955)
140. F. M. Peeters, J. T. Devreese: Phys. Rev. B **28**, 6051 (1983)
141. V. Cataudella, G. De. Filippis, C. A. Perroni: Single polaron properties in different electron phonon models, contribution to the present book.
142. E. G. Brovman, Yu. Kagan: Zh. Eksp. Teor. Fiz. **52**, 557 (1967) [Sov. Phys. JETP **25**, 365 (1967)]
143. K. A. Kikoin, A. S. Mishchenko: Zh. Eksp. Teor. Fiz. **104**, 3810 (1993) [Sov. Phys. JETP **77**, 828 (1993)]
144. B. Gerlach, H. L'owen: Rev. Mod. Phys. **63**, 63 (1991)
145. A. Brillante, M. R. Philpott: J. Chem. Phys. **72**, 4019 (1980)
146. D. Haarer: Chem. Phys. Lett. **27**, 91 (1974)
147. D. Haarer: J. Chem. Phys. **67**, 4076 (1977)
148. M. Kuwata-Gonokami, N. Peyghambarian, K. Meissner et al: Nature **367**, 47 (1994)

149. S. Curnoe, K. A. Kikoin: Phys. Rev. B **61**, 15714 (2000)
150. K. A. Kikoin, A. S. Mishchenko: Zh. Eksp. Teor. Fiz. **94**, 237 (1988) [Sov. Phys. JETP **67**, 2309 (1988)]
151. K. A. Kikoin, A. S. Mishchenko: J. Phys.: Condens. Matter **2**, 6491 (1990)
152. P. A. Alekseev, A. S. Ivanov, B. Dorner et al: Europhys. Lett. **10**, (1989) 457.
153. A. S. Mishchenko, K. A. Kikoin: J. Phys.: Condens. Matter **3**, 5937 (1991).
154. G. Trawaglini P. Wachter: Phys. Rev. B **29**, 893 (1984)
155. P. Lemmens, A. Hoffman, A. S. Mishchenko et al: Physica B **206&207**, 371 (1995)
156. T. Kasuya: Europhys. Lett. **26**, 277 (1994)
157. T. Kasuya: Europhys. Lett. **26**, 283 (1994)
158. E. Manousakis: Rev. Mod. Phys. **63**, 1 (1991)
159. E. Dagotto: Rev. Mod. Phys. **66**, 763 (1994)
160. P. A. Lee, N. Nagaosa, X. G. Wen: Rev. Mod. Phys. **78**, 17 (2006)
161. B. Batlogg, R. J. Cava, A. Jayaraman et al: Phys. Rev. Lett. **58**, 2333 (1987)
162. O. Gunnarsson, M. Calandra, J. E. Han: Rev. Mod. Phys. **75**, 1085 (2003)
163. R. Khasanov, D. G. Eshchenko, H. Luetkens et.al: Phys. Rev. Lett. **92**, 057602 (2004)
164. L. Pintschovius, M. Braden: Phys. Rev. B, **60**, R15039 (1999).
165. C. Thomsen, M. Cardona, B. Gegenheimer et. al: Phys. Rev. B **37**, 9860 (1988)
166. V. G. Hadjiev, X. Zhou, T. Strohm, et. al: Phys. Rev. B **58**, 1043 (1998)
167. G. Khaliullin, P. Horsch: Physica C **282-287**, 1751 (1997)
168. O. Rösch, O. Gunnarsson: Phys. Rev. Lett. **93**, 237001 (2004)
169. A. Lanzara, P. V. Bogdanov, X. J. Zhou et al: Nature **412**, 510 (2001)
170. T. Cuk, F. Baumberger, D. H. Lu et al: Phys. Rev. Lett. **93**, 117003 (2004)
171. T. P. Devereaux, T. Cuk, Z.-X. Shen, N. Nagaosa: Phys. Rev. Lett. **93**, 117004 (2004)
172. R. J. McQueeney, Y. Petrov, T. Egami et al: Phys. Rev. Lett. **82**, 628 (1999)
173. A. V. Chubukov, M. R. Norman: Phys. Rev. B **70**, 174505 (2004)
174. M. Eschrig, M. R. Norman: Phys. Rev. Lett. **85**, 3261 (2000)
175. M. Eschrig, M. R. Norman: Phys. Rev. B **67**, 144503 (2003)
176. X. J. Zhou, T. Yoshida, A. Lanzara et al: Nature **423**, 398 (2003)
177. K. M. Shen, F. Ronnig, D. H. Lu et al: Phys. Rev. Lett. **93**, 267002 (2004)
178. T. Xiang, J. M. Wheatley: Phys. Rev. B **54**, R12653 (1996)
179. B. Kyung, R. A. Ferrell: Phys. Rev. B **54**, 10125 (1996)
180. J. J. M. Pothuisen¹, R. Eder¹, N. T. Hien et al: Phys. Rev. Lett. **78**, 717 (1997)
181. K. A. Chao, J. Spalek, A. M. Oles: J. Phys. C **10**, L271 (1977)
182. C. Gross, R. Joynt, T. M. Rice: Phys. Rev. B **36**, 381 (1987)
183. M. Brunner, F. F. Assaad, A. Muramatsu: Phys. Rev. B **62**, 15480 (2000).
184. V. I. Belinicher, A. L. Chernyshev, V. A. Shubin: Phys. Rev. B **53**, 335 (1996)
185. V. I. Belinicher, A. L. Chernyshev, V. A. Shubin: Phys. Rev. B **54**, 14914 (1996)
186. T. Tohyama, S. Maekawa: Superconductors Science and Technology **13**, R17 (2000)
187. J. Bala, A. M. Oleś, J. Zaanen: Phys. Rev. B **52** 4597 (1995)
188. S. Schmitt-Rink, C. M. Varma, A. E. Ruckenstein: Phys. Rev. Lett. **60**, 2793 (1988)
189. Z. Liu, E. Manousakis: Phys. Rev. B **44**, 2414 (1991)
190. Z. Liu, E. Manousakis: Phys. Rev. B **45**, 2425 (1992)

191. B. Bauml, G. Wellein, H. Fehske: Phys. Rev. B **58**, 3663 (1998)
192. A. Ramšak, P. Horsch, P. Fulde: Phys. Rev. B **46**, 14305 (1992)
193. B. Kyung, S. I. Mukhin, V. N. Kostur, R. A. Ferrell: Phys. Rev. B **54**, 13167 (1996)
194. F. Marsiglio F, A. E. Ruckenstein, S. Schmitt-Rink, C. Varma: Phys. Rev. B **43**, 10882 (1991)
195. G. Martinez, P. Horsch: Phys. Rev. B **44**, 317 (1991)
196. O. Rösch, O. Gunnarsson: Phys. Rev. B **73**, 174521 (2006)
197. A. S. Mishchenko: Pis'ma Zh. Eksp. Teor. Fiz. **66**, 460 (1997) [JETP Lett. **66**, 487 (1997)]
198. O. Rösch, O. Gunnarsson: Europhys. Phys. J. B **43**, 11 (2005)
199. G. Sangiovanni, O. Gunnarsson, E. Koch, C. Castellani, M. Capone: cond-mat/0602606.
200. O. Rösch, O. Gunnarsson: Phys. Rev. B **70**, 224518 (2004).
201. G.-H. Gweon, T. Sasagawa, S. Y. Zhou et al: Nature **430**, 187 (2004)
202. O. Rösch, O. Gunnarsson, X. J. Zhou et al: Phys. Rev. Lett. **95**, 227002 (2005)
203. G. A. Sawatzky: Nature (London) **342B**, 480 (1989)
204. O. Rösch, O. Gunnarsson: Phys. Rev. Lett. **92**, 146403 (2004)
205. S. Ishihara , N. Nagaosa: Phys. Rev. B **69**, 144520 (2004)